

# 3D Photo-Fabrication for Tissue Engineering and Drug Delivery

Rúben F. Pereira<sup>1,2,3,4</sup> and Paulo J. Bártolo<sup>1,5,6\*</sup>

**ABSTRACT** The most promising strategies in tissue engineering involve the integration of a triad of biomaterials, living cells, and biologically active molecules to engineer synthetic environments that closely mimic the healing milieu present in human tissues, and that stimulate tissue repair and regeneration. To be clinically effective, these environments must replicate, as closely as possible, the main characteristics of the native extracellular matrix (ECM) on a cellular and subcellular scale. Photo-fabrication techniques have already been used to generate 3D environments with precise architectures and heterogeneous composition, through a multi-layer procedure involving the selective photocrosslinking reaction of a light-sensitive prepolymer. Cells and therapeutic molecules can be included in the initial hydrogel precursor solution, and processed into 3D constructs. Recently, photo-fabrication has also been explored to dynamically modulate hydrogel features in real time, providing enhanced control of cell fate and delivery of bioactive compounds. This paper focuses on the use of 3D photo-fabrication techniques to produce advanced constructs for tissue regeneration and drug delivery applications. State-of-the-art photo-fabrication techniques are described, with emphasis on the operating principles and biofabrication strategies to create spatially controlled patterns of cells and bioactive factors. Considering its fast processing, spatiotemporal control, high resolution, and accuracy, photo-fabrication is assuming a critical role in the design of sophisticated 3D constructs. This technology is capable of providing appropriate environments for tissue regeneration, and regulating the spatiotemporal delivery of therapeutics.

**KEYWORDS** 3D photo-fabrication, biomaterials, tissue engineering, drug delivery

## 1 Introduction

In the past two decades, the field of tissue engineering has

experienced significant advances in multiple areas (e.g., isolation of novel cell sources, synthesis of advanced biomaterials with high levels of biomimicry, discovery of new drugs, and development of high throughput biofabrication strategies), resulting in the development of innovative clinical therapies to stimulate the repair and regeneration of injured tissues with better clinical outcomes [1–7]. Current therapies in tissue engineering and regenerative medicine can be broadly categorized into three main groups: ① cell-based therapy, ② acellular or cell-seeded scaffold therapy, and ③ the implantation of cell-laden constructs/matrices (Figure 1).

In cell-based therapy, autologous, allogenic, or heterologous cells are harvested from the patient (autologous) or a donor (allogenic, heterologous), and submitted to a set of processing steps (e.g., cell sorting, *in vitro* expansion) for subsequent implantation into the lesion [8]. Despite the relative simplicity of this therapy, it faces major difficulties in maintaining the administered cells in the desired location for clinically relevant periods of time, without a decrease of cell viability post-injection. Alternatively, cells might be immobilized within polymeric vehicles in order to improve the residence time in the target, and enhance the clinical efficacy [9]. Depending on the dimension of the injury and the biomechanical characteristics of the tissue, the implantation of a scaffold material may be the best option, as it provides a temporary environment that guides the infiltration, colonization, attachment, and proliferation of either seeded or host cells, promoting the synthesis of new extracellular matrix [1, 10]. To stimulate the reparative process in an appropriate way, scaffolds must fulfill a series of classical physicochemical, mechanical, and biological requisites, including biocompatibility, bioreabsorbability, non-cytotoxicity, appropriate stiffness, elasticity, and surface properties [1, 10, 11]. Scaffold characteristics are primarily determined by the nature and chemistry of the selected biomaterial. Natural and synthetic polymers are the most widely used biomaterials, allowing the fabrication of scaffolds with a wide range of bioactivity, biomimicry, bio-

<sup>1</sup> Centre for Rapid and Sustainable Product Development (CDRsp), Polytechnic Institute of Leiria, Marinha Grande 2430-028, Portugal; <sup>2</sup> Instituto de Investigação em Inovação em Saúde (I3S), Universidade do Porto, Porto 4200-393, Portugal; <sup>3</sup> Instituto Nacional de Engenharia Biomédica (INEB), Universidade do Porto, Porto 4150-180, Portugal; <sup>4</sup> Instituto de Ciências Biomédicas Abel Salazar (ICBAS), Universidade do Porto, Porto 4050-313, Portugal; <sup>5</sup> School of Mechanical, Aerospace and Civil Engineering, University of Manchester, Manchester M13 9PL, UK; <sup>6</sup> Manchester Institute of Biotechnology, University of Manchester, Manchester M1 7DN, UK

\* Correspondence author. E-mail: paulojorge.dasilvabartolo@manchester.ac.uk

Received 5 March 2015; received in revised form 25 March 2015; accepted 25 March 2015

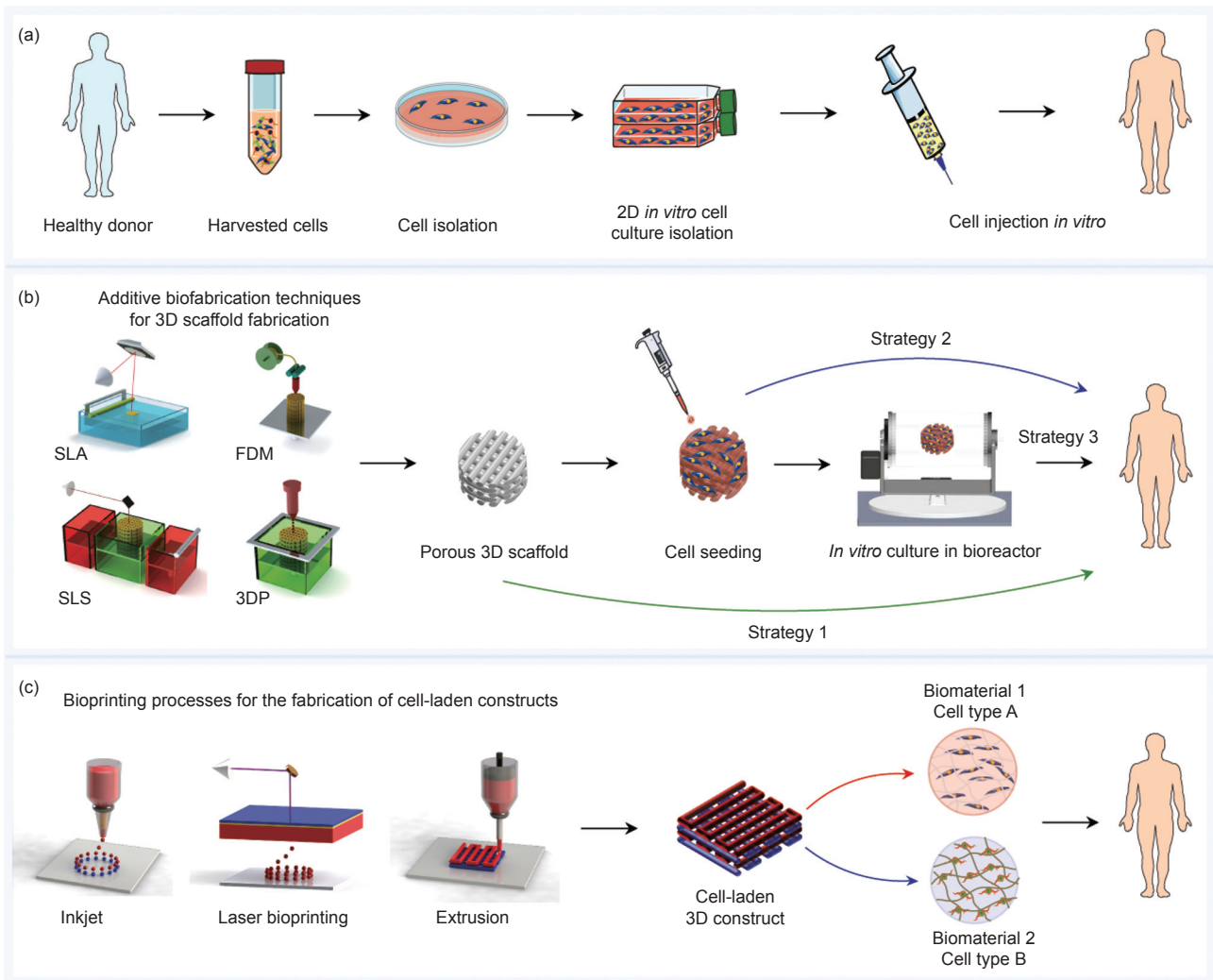


**Figure 1. Main therapies for tissue engineering and regenerative medicine.** (a) Cell-based therapy; (b) scaffold-based therapy; (c) therapy based on the implantation of cell-laden 3D constructs. In scaffold-based therapy, scaffolds can be implanted without cells (Strategy 1), after cell seeding (Strategy 2), or upon *in vitro* culture (Strategy 3). For simplicity, traditional biofabrication techniques to produce 3D scaffolds were not considered in this work.

degradation, and cell interactive properties [12]. For certain applications, such as bone or osteochondral tissue engineering, polymeric scaffolds are usually reinforced with bioactive ceramic materials (e.g., hydroxyapatite or  $\beta$ -tricalcium phosphate), in order to achieve better mineralization and integration into the host [13, 14]. In addition to the nature of the biomaterial, the biofabrication technique also determines key features of the scaffold (e.g., pore size, shape and interconnectivity, internal architecture, micro and macroporosity, surface topography, and spatial distribution of pores) at a macro, micro, and nanometric scale, strongly influencing the *in vitro* cell behavior and the *in vivo* tissue formation [15–17]. To date, a multitude of biofabrication techniques is available to produce two-dimensional (2D) and three-dimensional (3D) matrices for scaffold-based therapy. Traditional biofabrication techniques, such as solvent casting, freeze drying, or gas foaming, are still applied in the fabrication of porous scaffolds from a variety of biomaterials. This continued use is mainly due to their simplicity and low cost, since they do not require any sophisticated machinery. However, they provide limited control over the internal architecture (e.g., porosity, pore size, spatial distribution, and interconnectivity of pores),

imposing severe restrictions on the introduction of spatial variations of biomaterials throughout the scaffold [10, 18]. Another important limitation is the impossibility of including living cells and signaling molecules during fabrication, due to the presence of non-compatible solvents, lengthy timescales, and harsh conditions [18]. In contrast, additive biofabrication techniques, such as stereolithography (SLA), selective laser sintering (SLS), melt extrusion or fused deposition modeling (FDM), and inkjet printing or 3D printing (3DP), enable the fabrication of scaffolds with enhanced accuracy, resolution, and reproducibility [1, 19]. Using these techniques, 3D scaffolds are automatically generated through a layer-by-layer approach, remarkably increasing the complexity and heterogeneity of the fabricated structures. Additive technologies allow for integration with medical-image systems, and provide better control over scaffold properties. However, major drawbacks still persist in these technologies regarding the non-homogeneous seeding of cells, insufficient vascularization, and heterogeneous tissue growth [20]. Therapies based on the implantation of cell-laden matrices appear to be promising alternatives to address the limitations of cell- and scaffold-based modalities, through the direct fabrication of

heterogeneous 3D environments organized at different length scales [21]. In these therapies, a group of biofabrication technologies capable of manipulating a plethora of biomaterials, cells, and signaling molecules are employed to generate specialized environments that recapitulate the native ECM of the target tissue, not only from a structural point of view but also from a biochemical perspective [20, 22]. These technologies, known as bioprinting, are recognized as a key tool in tissue engineering. They enable the rapid fabrication of complex constructs through a controlled layer-by-layer deposition of prepolymer solutions, suspended cells, cell aggregates, and biologically active molecules (referred as “bioink”) onto a receiving substrate (known as “biopaper”) [18, 22]. Bioprinting has been successfully applied in the fabrication of cell-laden constructs with enhanced levels of heterogeneity, which simultaneously act as scaffolds to accommodate embedded cells and platforms for the delivery of therapeutic molecules [23].

Among the biofabrication techniques currently being applied to produce 3D constructs for biomedical applications, photo-fabrication technologies have been attracting increasing interest, due to their excellent resolution, accuracy, and ability to precisely manipulate biomaterials, cells, and therapeutic molecules in 3D environments [24]. In photo-fabrication technologies, a variety of light-induced reactions, such as photopolymerization, photopatterning, and photodegradation, are employed to promote the synthesis of hydrogels (photopolymerization) and/or to introduce biochemical or mechanical changes in the hydrogel network (photopatterning and photodegradation). The light-induced reactions involved in photo-fabrication allow *in situ* crosslinking of photosensitive polymers in the presence of cells and bioactive molecules, providing great control over the spatiotemporal formation of the hydrogel [25, 26]. These technologies are also very attractive due to their ability to manipulate hydrogel features in real time with micron-scale resolution (e.g., altering gel crosslinking density, locally cleaving photosensitive bonds, and patterning biological functionalities), providing further control over cell functions (e.g., migration and proliferation) and the release of biochemical ligands [24, 27, 28]. This review paper focuses on recent developments in 3D photo-fabrication strategies for tissue regeneration and the delivery of therapeutics. The next section describes the key elements of light-sensitive systems, focusing on photopolymerization schemes, photoinitiators, and strategies to introduce reactive functional groups into the polymer chain. Subsequent sections emphasize the photo-fabrication techniques used to engineer 3D constructs for biomedical applications.

## 2 Engineering photosensitive systems for biofabrication

Photosensitive systems can be defined as polymer-based formulations that respond to an external light stimulus, through a series of changes in their physical, chemical, or mechanical characteristics. Photopolymerization and photodegradation reactions are commonly used to trigger changes in a photosensitive system and to produce 3D structures.

Photopolymerization is one of the most explored methods of creating covalently crosslinked hydrogels, through the exposure of a photosensitive system composed of unsaturated prepolymers, photoinitiators, and other compounds such as cells and therapeutic molecules, to ultraviolet (200–400 nm) or visible light (400–800 nm) [25, 29]. The use of light energy affords the rapid *in situ* formation of hydrogels (occurring in timescales of seconds to a few minutes), under biocompatible reaction conditions and low initiating radical doses. This rapid formation provides facile control over the spatiotemporal formation of the gel at relevant length scales [25, 30, 31]. The resolution and spatiotemporal control conferred by the light are important not only to induce the hydrogel crosslinking, but also to ① promote the local cleavage of photosensitive bonds [32], ② introduce specific biochemical functionalities in 3D environments [27], and ③ assist in the printing of cellular bioinks [33].

### 2.1 Photopolymerization reactions

Photopolymerization reactions used for the synthesis of biocompatible hydrogels can be classified into free-radical-initiated chain polymerization and bio-orthogonal click reactions [34].

Free-radical photopolymerization, based on (meth)acrylate functionalized prepolymers and occurring through a chain-growth mechanism (Figure 2), is the most popular method for producing hydrogels. The incident light energy (photons) that is absorbed by the photoinitiators triggers the formation of free radicals that react with the vinyl bonds present in the prepolymer, promoting the establishment of chemical crosslinks between the polymer chains [35]. This polymerization reaction permits the synthesis of hydrogels from a variety of natural and synthetic polymers, resulting in hydrogels with tunable mechanical, degradation, and biological properties. Hydrogels can also be further functionalized with cell adhesive moieties and degradation sites in a relatively easy and reproducible manner [36, 37]. However, radical-initiated chain-growth polymerization has several limitations, including: ① relatively poor control over the crosslinking kinetics, ② oxygen inhibition, ③ the presence of unreacted double bonds that might potentially react with biological substances, and ④ the generation of heterogeneities within the polymer network, due to the random chain polymerization [30, 34, 38, 39]. On the other hand, bio-orthogonal click reactions are characterized by orthogonal reactivity and the step-growth mechanism of the polymerization reaction, enabling the fabrication of structurally uniform hydrogels with minimal network defects [30, 34, 38, 39]. In addition, click chemistry is insensitive to water and oxygen, and can proceed under mild reaction conditions with higher efficiency, selectivity, and faster kinetics when compared to free-radical polymerization [27, 39, 40].

Among the myriad of existing bio-orthogonal click schemes, the thiol-norbornene (thiol-ene) photoclick reaction has emerged as a powerful method for engineering biocompatible hydrogels. This reaction involves light-mediated orthogonal reactions between multifunctionalized macromers that are end-capped with norbornene functionalities

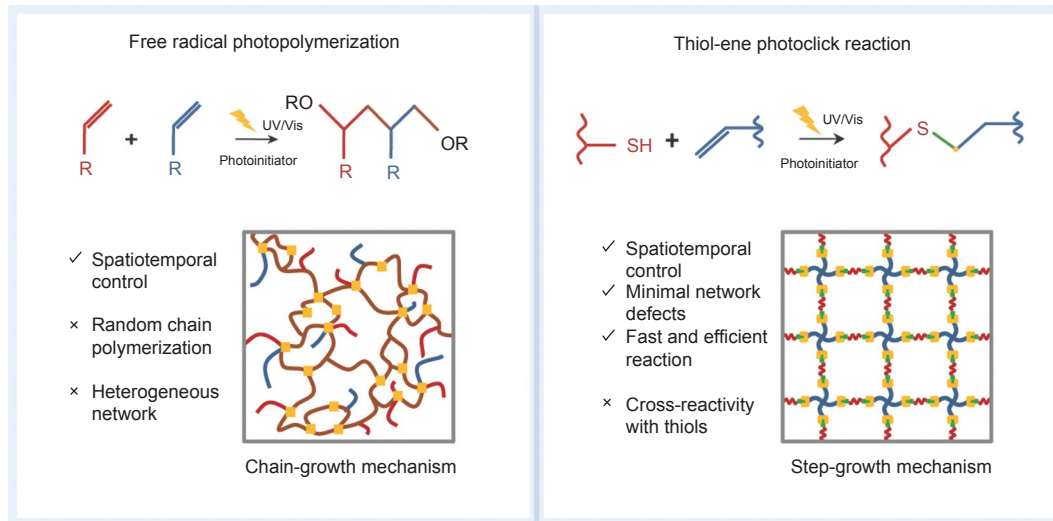


**Figure 2.** Light-mediated polymerization reactions to engineer hydrogels for tissue engineering.

and sulfhydryl-containing linkers, in the presence of low amounts of photoinitiator [34, 39–41]. Under UV or visible light irradiation, the thiol-ene reaction promotes the rapid radical-mediated addition of thiols (e.g., bis-cysteine peptides and dithiothreitol) to carbon-carbon double bonds within functionalized prepolymers (e.g., norbornene-functionalized four-arm poly(ethylene glycol) (PEG)), yielding thioether bonds without inducing cytotoxic effects to the encapsulated cells (Figure 2) [27, 42, 43]. Like free-radical polymerization, the thiol-ene reaction is photochemically controlled and affords the localized covalent tethering of pendant matrix metalloproteinase (MMP)-degradable and/or adhesive peptide sequences, resulting in enhanced control of hydrogel degradation, cell fate, and cell-matrix interactions [27]. Radical-mediated thiol-norbornene photopolymerization can also be performed in both acellular and cell-laden hydrogels, for manipulating the biomechanical and biochemical characteristics of the hydrogels [44].

## 2.2 Cytocompatible photoinitiators

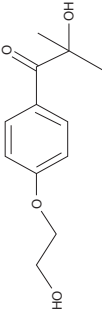
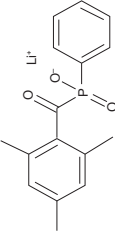
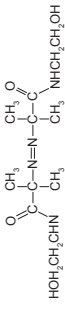
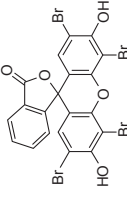
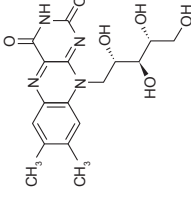
The selection of a suitable photoinitiator is a prime requisite to ensure an adequate polymerization rate and to avoid cytotoxic effects for both embedded cells and surrounding tissues. When selecting a photoinitiator, key characteristics should be considered, including water solubility, stability, absorption spectrum, molar absorptivity, and efficiency in generating free radicals [25, 43]. Currently available photoinitiators can be divided into two main categories: radical or cationic [45]. Radical photoinitiators are the most used, due to their superior biocompatibility. On the other hand, the use of cationic photoinitiators results in the formation of protonic acids, making these photoinitiators less useful in biomedical applications [25]. According to the mechanism involved in the generation of free radicals, radical photoinitiators can be further categorized as photo-cleavable photoinitiators (type I) or bimolecular photoinitiators (type II). Upon light exposure, type I photoinitiators (e.g., benzoin derivatives, benzyl ketal, acetophenone derivatives, hydroxyalkylphenones, and acylphosphine oxides) absorb incident photons and decom-

pose into two primary radicals that initiate the crosslinking, whereas type II photoinitiators (e.g., benzophenone, camphorquinone, and thioxanthone) abstract the hydrogen from a co-initiator to generate secondary radicals for crosslinking [43, 45]. Although type I initiators are usually the first choice because of their superior initiation efficiency [39], recently there has been an increasing interest in type II initiators for visible-light-mediated polymerization (Table 1). The main concern associated with the use of light-mediated polymerization for cell encapsulation is the potential cytotoxicity of free radicals generated by photoinitiators. During photopolymerization, free radicals can react with cellular components (e.g., cell membrane, nucleic acids, or proteins) via either direct contact or the formation of reactive oxygen species, which may compromise the viability of embedded cells, and even lead to DNA damage [26, 46]. The cytotoxic effects of several photoinitiators on both primary cells and cell-lines are well-documented in the literature, and strongly depend on the photoinitiator type and concentration, exposure time, and light intensity [26, 46–49]. Irgacure 2959 (1-[4-(2-hydroxyethoxy)-phenyl]-2-hydroxy-2-methyl-1-propane-1-one) is the most commonly used photoinitiator, due to its moderate water solubility and low cytotoxicity. However, its low molar extinction coefficient in the UV-A spectral range, and its low initiation efficiency, boosted the research on alternative photoinitiators exhibiting enhanced biocompatibility and/or efficiency, such as 2,2'-azobis[2-methyl-N-(2-hydroxyethyl)propionamide] (VA-086) and lithium phenyl-2,4,6-trimethylbenzoylphosphine (LAP) [47, 50–52]. In parallel to this work, researchers concentrated efforts on the formulation of photopolymerizable systems containing visible-light-sensitive photoinitiators (e.g., camphorquinone, riboflavin, and Eosin-Y), in order to mitigate potential deleterious effects of UV light on the encapsulated cells [43, 53].

## 2.3 Designing advanced biomaterials for light-mediated reactions

The design of hydrogel precursors for light-mediated reactions, including photopolymerization, photodegradation, and photopatterning, involves the consideration of a plethora of

Table 1. Summary of the most common photoinitiators for photo-fabrication and examples of polymerization systems currently used for cell encapsulation.

| Name       | Type | Chemical structure                                                                    | Photopolymerizable system                                                                      |                                                                                                                                                                               |                                                                                                                                      |                                                                                                                                                                          | Reference                                                                                    |              |
|------------|------|---------------------------------------------------------------------------------------|------------------------------------------------------------------------------------------------|-------------------------------------------------------------------------------------------------------------------------------------------------------------------------------|--------------------------------------------------------------------------------------------------------------------------------------|--------------------------------------------------------------------------------------------------------------------------------------------------------------------------|----------------------------------------------------------------------------------------------|--------------|
|            |      |                                                                                       | Photopolymerization reaction                                                                   | Irradiation conditions                                                                                                                                                        | Hydrogel precursor                                                                                                                   | Encapsulated cells                                                                                                                                                       |                                                                                              |              |
| I2959      | I    |    | Free-radical polymerization<br>Thiol-ene click chemistry                                       | UV light (360–480 nm),<br>6.9 mW·cm <sup>-2</sup> , 15 s<br><br>UV light, 10 mW·cm <sup>-2</sup> ,<br>30 s                                                                    | Gelatin methacrylate,<br>0.5% (w/v) I2959<br><br>HA-norbormene, DTT,<br>0.05 wt.% I2959                                              | NIH 3T3 fibroblasts<br>(5 × 10 <sup>6</sup> cells·mL <sup>-1</sup> )<br><br>hMSCs (1 × 10 <sup>7</sup> cells·mL <sup>-1</sup> )                                          | 75%–92%, 8 h post-<br>encapsulation<br><br>96% (1 d) and<br>88% (3 d) post-<br>encapsulation | [54]<br>[55] |
| LAP        | I    |    | Free-radical polymerization<br>Thiol-ene click chemistry                                       | Visible light (405 nm)/UV<br>light (365 nm)<br>10 mW·cm <sup>-2</sup> , 5 min<br><br>UV light (365 nm),<br>5 mW·cm <sup>-2</sup> , 2 min                                      | PEGDA, 2,2/<br>0.22 mmol·L <sup>-1</sup> LAP<br><br>PEG-norbormene,<br>0.05 wt.% LAP                                                 | Human neonatal<br>fibroblast<br>(1 × 10 <sup>6</sup> cells·mL <sup>-1</sup> )<br><br>hMSCs (5 × 10 <sup>6</sup> cells·mL <sup>-1</sup> )                                 | >95%, 24 h post-<br>encapsulation<br><br>Cells survive, 14 d<br>post-encapsulation*          | [51]<br>[36] |
| VA-086     | I    |    | Free-radical polymerization                                                                    | UV light (365 nm),<br>2 mW·cm <sup>-2</sup> , 5 min                                                                                                                           | Alginate<br>Methacrylate, 0–1.5% (w/v)<br>VA-086                                                                                     | Bovine articular<br>chondrocytes<br>(50 × 10 <sup>6</sup> cells·mL <sup>-1</sup> )                                                                                       | >90%, 48 h post-<br>encapsulation                                                            | [47]         |
| Eosin-Y    | II   |   | Mixed mode (chain and step-<br>growth reactions) <sup>§</sup><br><br>Thiol-ene click chemistry | UV light (365 nm),<br>4 mW·cm <sup>-2</sup> , 1800 mJ·cm <sup>-2</sup><br><br>Visible light (525 nm),<br>5 mW·cm <sup>-2</sup> (7 min) /<br>100 mW·cm <sup>-2</sup> (1.5 min) | Gelatin methacrylamide,<br>20 mol% VA-086<br><br>PEGDA, Thiolated<br>heparin, TEOA, 0.01%<br>Eosin-Y                                 | HepG2 cells<br>(1.5 × 10 <sup>6</sup> cells·mL <sup>-1</sup> )<br><br>NIH 3T3 fibroblasts<br>(2 × 10 <sup>6</sup> cells·mL <sup>-1</sup> )                               | >95%, 24 h post-<br>encapsulation<br><br>>96%                                                | [50]<br>[56] |
| Riboflavin | II** |  | Free-radical polymerization                                                                    | Visible light (780 nm<br>femtosecond laser,<br>followed by 1 min at 570<br>nm light)<br><br>Visible light (515 nm),<br>10 mW·cm <sup>-2</sup> , 4 min                         | PEGDA, TEOA, 200 μmol·L <sup>-1</sup><br>riboflavin<br><br>Methacrylated glycol<br>chitosan/HA, 6 μmol·L <sup>-1</sup><br>Riboflavin | Bovine aortic endothelial<br>cells (1 × 10 <sup>6</sup> cells·mL <sup>-1</sup> )<br><br>Human<br>mesenchymal stem cells<br>(5 × 10 <sup>6</sup> cells·mL <sup>-1</sup> ) | ~95%, 14 h post-<br>encapsulation<br><br>>90%, after 24 h <sup>§§</sup>                      | [43]<br>[57] |
|            |      |                                                                                       | Free-radical polymerization                                                                    | Visible light 400–500 nm),<br>300 mW·cm <sup>-2</sup> , 120–600 s                                                                                                             |                                                                                                                                      | Auricular chondrocytes<br>(2 × 10 <sup>6</sup> cells·mL <sup>-1</sup> )                                                                                                  | 60%–90%, 24 h<br>post-encapsulation <sup>#</sup>                                             | [58]         |

**Notes:** Irgacure 651 (2,2-dimethoxy-2-phenylacetophenone); PEG4NB (poly(ethylene glycol)-tetra-norbormene); PEG (poly(ethylene glycol)); PEGDA (poly(ethylene glycol) Diacrylate); HA (hyaluronic acid); TEOA (triethanolamine); NVP (1-vinyl-2-pyrrolidone); hMSCs (Human mesenchymal stem cells); DTT (dithioeritol); HepG2 (hepatocarcinoma cell line). <sup>§</sup>Quantitative data about cell viability is not available, but authors reported that cells survived and retain differentiation ability. <sup>\*\*</sup>Riboflavin can form either singlet or triplet-excited states upon light absorption. <sup>#</sup>Authors state a predominance of thiol-ene reaction and negligible acrylate polymerization rates. <sup>§§</sup>Cell viability was assessed by culturing cells in the presence of photopolymer extract solutions, instead of cell encapsulation. <sup>#</sup>Depending on the irradiation time and presence of HA.

physicochemical, mechanical, and biological features that determine the processing and performance of the hydrogel, as shown in Figure 3 [29, 59].

Hydrogels have been extensively explored in tissue engineering and drug delivery, due to the availability of numerous crosslinking schemes and to the unique ability of hydrogels to resemble some features of natural ECM [31, 60]. Cell-compatible hydrogels can be prepared using polymeric materials of natural or synthetic origin [60]. Naturally derived polymers retain inherent biochemical similarities with the natural ECM matrix, providing biological recognition properties, cell-triggered degradation, and remodeling; however, major concerns arise from the complex purification processes, batch-to-batch variability, limited mechanical properties, and potential immunogenicity [35]. On the other hand, synthetic polymers are assuming a central position in modern healthcare therapies because of their controllable properties, superior mechanical performance, and possibility for obtaining multifunctional hydrogels with tunable properties [61]. However, pure synthetic polymers often exhibit limited biocompatibility, biodegradability, and cell-interaction properties [35]. To circumvent these limitations, synthetic polymers are usually functionalized with a number of biological motifs (e.g., cell-proteolytic domains and/or cell adhesion sites) that provide control over the hydrogel degradation, cell fate, and tissue remodeling [27]. Although polymers, whether natural or synthetic, have several functional groups (e.g., COOH, NH<sub>2</sub>, and OH) in

their chemical structure, most do not contain photoreactive moieties, which precludes the occurrence of light-mediated reactions [62]. Thus, the design of hydrogel precursors for light-mediated chemistries primarily involves the chemical modification of prepolymers with reactive pendant groups (e.g., acrylates, methacrylates, or norbornene), which must be selected according to both the photopolymerization scheme to be used and their inherent cytotoxicity, reactivity, and biodegradability. The type and number of reactive groups to be introduced into the polymer backbone should also be carefully optimized, to prevent dramatic changes in the physicochemical properties of the polymer (e.g., hydrophilicity, charge, water solubility, elasticity, mesh size, and diffusivity), which may ultimately impair the hydrogel cytocompatibility, biodegradability, and bioactivity. In the next sections, we briefly describe the most common reactive groups and chemical pathways for engineering hydrogel precursors for light-mediated reactions.

### 2.3.1 Hydrogel precursors for free-radical polymerization

Hydrogel precursors for free-radical polymerization are synthesized by introducing vinyl groups into the backbone of natural and synthetic polymers, via chemical modification with acrylates, methacrylates, fumarates, and vinyl esters, as summarized in Table 2. It is widely accepted that acrylates possess the highest reactivity, followed by vinyl ester, vinyl carbonate, vinyl carbamate, methacrylate, and fumarate derivatives [63, 64]. Although the reactivity of acrylates

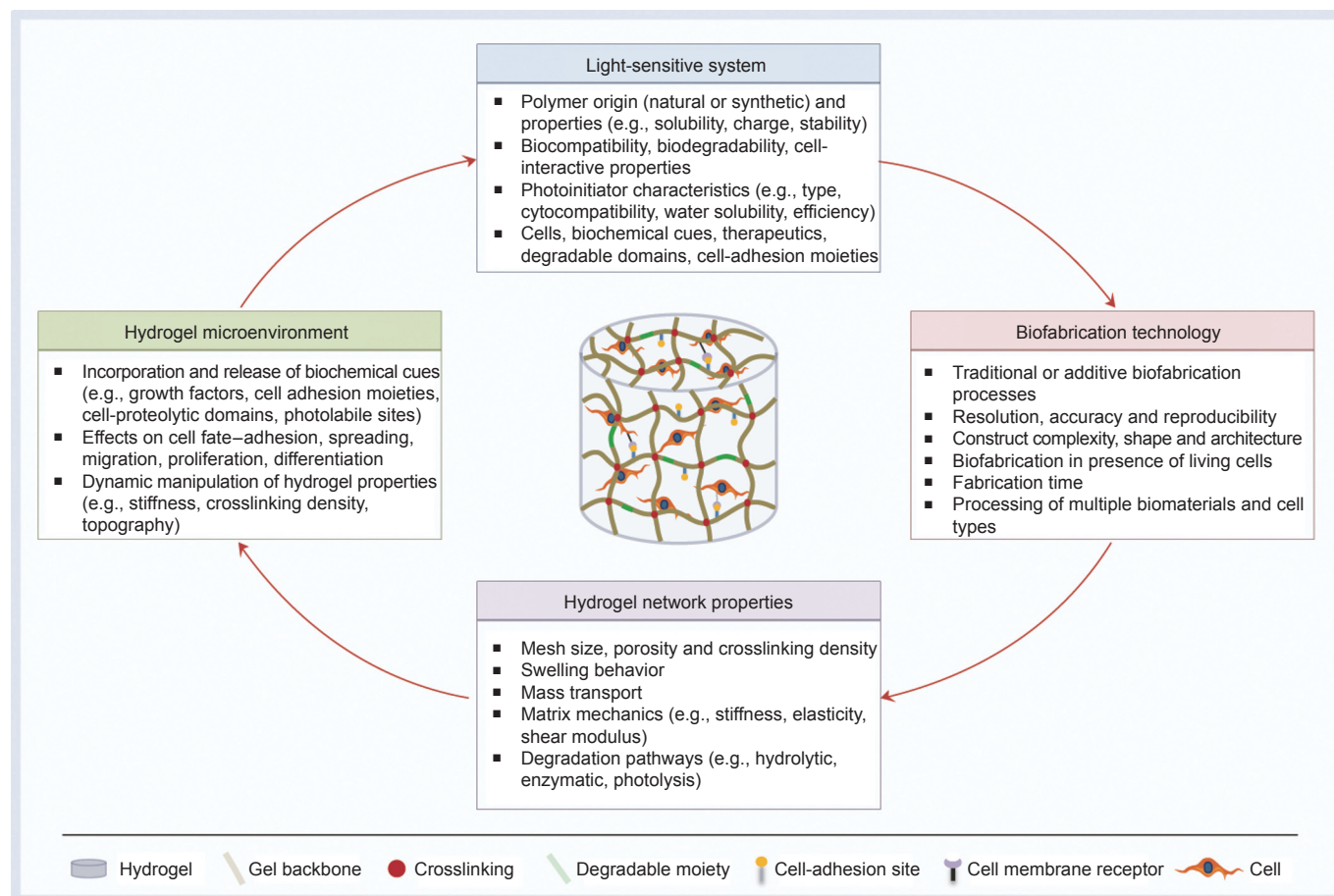
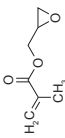
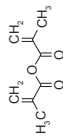


Figure 3. Design considerations when engineering biocompatible and biodegradable hydrogels through light-mediated polymerization reactions.

Table 2. Most commonly applied reactive groups in the engineering of hydrogel precursors for light-mediated reactions.

| Reactive group      | Commercial Reagent          | Chemical structure                                                                  | Hydrogel precursors                                                                      | Light-mediated reaction              | Application                                                                    | Reference |
|---------------------|-----------------------------|-------------------------------------------------------------------------------------|------------------------------------------------------------------------------------------|--------------------------------------|--------------------------------------------------------------------------------|-----------|
| Methacrylate        | Glycidyl methacrylate (GMA) |  | Hyaluronic acid                                                                          | Free-radical photopolymerization     | Tissue engineering and cell encapsulation                                      | [69]      |
|                     | Methacrylic anhydride (MA)  |  | Glycol chitosan                                                                          | Free-radical photopolymerization     | Cartilage tissue engineering, cell encapsulation                               | [53]      |
|                     |                             |                                                                                     | Gelatin                                                                                  | Free-radical photopolymerization     | Tissue engineering, cell encapsulation and bioprinting                         | [50]      |
|                     |                             |                                                                                     | Alginate                                                                                 | Free-radical photopolymerization     | Cell encapsulation                                                             | [47]      |
| Acrylate            |                             |                                                                                     | Hyaluronic acid                                                                          | Free-radical photopolymerization     | Cell encapsulation                                                             | [68]      |
|                     |                             |                                                                                     | Tropoelastin                                                                             | Free-radical photopolymerization     | Tissue engineering and cell encapsulation                                      | [74]      |
|                     |                             |                                                                                     | Heparin                                                                                  | Free-radical photopolymerization     | Growth factor delivery                                                         | [67]      |
|                     |                             |                                                                                     | Hyaluronic acid                                                                          | Free-radical photopolymerization     | Drug delivery                                                                  | [75]      |
| Norbornene          |                             |                                                                                     | Dextran                                                                                  | Free-radical photopolymerization     | Drug delivery                                                                  | [66]      |
|                     |                             |                                                                                     | PEG                                                                                      | Free-radical photopolymerization     | Cell encapsulation                                                             | [51]      |
|                     |                             |                                                                                     | Hyperbranched polyester                                                                  | Free-radical photopolymerization     | Drug delivery                                                                  | [76]      |
|                     |                             |                                                                                     | 4-arm PEG                                                                                | Thiol-norbornene photopolymerization | Cell encapsulation and peptide photopatterning                                 | [44]      |
| o-nitrobenzyl ester |                             |                                                                                     | Hyaluronic acid                                                                          | Thiol-norbornene photopolymerization | Cell encapsulation and peptide photopatterning                                 | [55]      |
|                     |                             |                                                                                     | Gelatin                                                                                  | Thiol-norbornene photopolymerization | Cell encapsulation                                                             | [77]      |
|                     |                             |                                                                                     | Gelatin methacrylamide, photodegradable PEG                                              | Photodegradation                     | Photopatterning and cell manipulation                                          | [32]      |
|                     |                             |                                                                                     | Dextran functionalized with acrylate-modified o-nitrobenzyl moieties and dithiolated PEG | Photodegradation                     | Protein delivery                                                               | [78]      |
| Coumarin            |                             |                                                                                     | 4-armed PEG tetracarboxylic acid                                                         | Photodegradation                     | Tissue engineering and spatiotemporal patterning of cellular microenvironments | [72]      |
|                     |                             |                                                                                     | PEG-DBCO, PEG-N <sub>3</sub>                                                             | Photodegradation                     | Protein delivery                                                               | [73]      |

Notes: PEG-DBCO (PEG tetra-dibenzocyclooctyne); PEG-N<sub>3</sub> (4-armed PEG tetraazide); BMP (bone morphogenetic protein). \*Synthesized using commercially available 7-amino-4-methylcoumarin. \*\*Synthesized from commercially available acetovanillone.

enables high reaction kinetics and double-bond conversion, the cytotoxicity and skin irritancy of acrylates still remain as major pitfalls for biomedical applications [64]. On the other hand, the main limitation of methacrylates is their limited reactivity, as a result of the sterical hindrance and inductive stabilization of radicals from the methyl group [65]. The skin irritancy can be significantly reduced by ensuring an almost complete consumption of double bonds, avoiding non-specific reactions with the amino or thiol groups in proteins. Cytotoxicity has been mainly addressed by the development of alternative monomers, particularly those based on vinyl esters [63, 65]. Photopolymerizable monomers based on vinyl esters were synthesized by Heller, exhibiting superior biocompatibility in the presence of the MC3T3-E1 cell line, when compared to acrylate- and methacrylate-modified polymers. These researchers also showed that susceptibility to *in vitro* degradation occurs in the following order: vinyl ester > acrylate > vinyl carbonate > methacrylate > vinyl carbamate [63, 65].

One of the most widespread chemical modifications consists of the (meth)acrylation of polymers, through a reaction with glycidyl methacrylate, methacrylic anhydride, or acryloyl chloride. Depending on the polymer chemistry and reactive agent, the esterification reaction proceeds predominantly through the primary hydroxyl groups [66], carboxylic groups [67], and amine side groups [54] of the polymer, under either homogeneous or heterogeneous conditions. Although homogeneous conditions are usually the first choice for the modification of natural polymers, because of their hydrophilic nature [47, 50], reactive agents easily hydrolyze under these conditions. Alternatively, natural polymers can be converted to a tetrabutylammonium (TBA) salt in order to allow dissolution in organic solvents [68], or reacted under heterogeneous conditions by using a co-solvent mixture that reduces the hydrolysis of functionalizing agents and enhances the degree of modification [69].

### 2.3.2 Hydrogel precursors for thiol-ene click polymerization

Radical-mediated thiol-ene reactions also require the functionalization of naturally derived or synthetic polymers with reactive side groups. According to Tasdelen and Yagci [41], the rate of thiol-ene conjugation is determined by the chemical structure of alkenes, and the reaction with electron-rich and/or strained alkenes is faster than with electron-poor alkenes, following the order norbornene > vinyl ether > alkene > vinyl ester > allyl ether > acrylate > *N*-substituted maleimide > methacrylate > conjugated dienes. Due to their superior reactivity and ideal step-growth polymerization, norbornene monomers are the most popular reactive groups for photoinitiated thiol-ene reactions. Contrary to the step-growth polymerization of norbornene, reactive groups like acrylates and methacrylates result in the formation of hydrogel networks by a combination of chain- and step-growth polymerization, due to competing reactions between acrylate groups and thiol-ene coupling. However, a recent work argued that the formation of thiol-acrylate bonds predominates over the chain-growth homopolymerization of acrylate groups [56].

### 2.3.3 Hydrogel precursors for photodegradation and photopatterning reactions

Rather than simply triggering the establishment of chemical bonds between polymer chains to induce hydrogel formation, light-mediated reactions are also very attractive for promoting the spatiotemporal degradation of crosslinks (e.g., releasing therapeutics and reducing crosslinking) and inducing the real-time patterning of biochemical cues within hydrogels with micrometer-scale resolution.

The most common method of designing hydrogel precursors for photodegradation is based on the use of molecules containing nitrobenzyl ether moieties (e.g., *o*-nitrobenzyl ether), which undergo photolysis through the absorption of light in the UV and low visible light region, typically in the range of 280–450 nm [32, 70, 71]. However, the photolysis of nitrobenzyl moieties yields a nitroso ketone group and a carboxylic acid group capable of reacting with the amine moieties of proteins [32, 72]. This drawback was recently addressed through the use of coumarins as photodegradable motifs; these undergo photolysis under both single- and two-photon polymerization (2PP) irradiation, leading to the formation of a less-reactive alcohol as a byproduct [72].

The simpler approach for engineering hydrogel precursors for photopatterning reactions starts with the introduction of reactive functional groups into the polymer backbone according to the aforementioned strategies. Next, the functional groups that remain available (non-reacted) upon the hydrogel formation are exploited for secondary reactions (e.g., light-mediated peptide coupling), thereby avoiding complex and time-consuming chemical modifications [55]. In more complex approaches, hydrogel precursors can be specifically designed to incorporate photolabile, caged moieties (e.g., bone morphogenic protein-2 (BMP-2) and BMP-7 covalently modified with photocleavable azides) that remain unaltered (inactive) during the gel formation. Upon localized light exposure, the cages are released and the moieties reactivated for subsequent biomolecule tethering [28, 73]. Although this approach involves additional, complex chemical reactions, especially for the synthesis of caged moieties, it provides the possibility of engineering environments with site-specific tethering of fragile biochemical cues, placed in predefined 3D spatial locations within the gel, which react at a desired time.

## 3 3D photo-fabrication: From acellular scaffolds to spatiotemporally manipulated cell-laden constructs

3D photo-fabrication comprises a group of techniques that use light energy to trigger a series of chemical reactions in a photosensitive system, including single and 2PP stereolithography [10]. In a different approach, laser direct-write techniques, such as laser-guided direct write (LGDW) and modified-laser-induced forward transfer (modified-LIFT), employ light energy to generate radiation forces or local heating, respectively, that promote the ejection of bioinks toward a substrate [79, 80]. In both approaches, photo-fabrication enables the fabrication of personalized, complex 3D structures through a multi-step protocol that is fully implemented in additive biomanufacturing technologies, and starts with the



generation of a computer solid model. This model can be obtained by computer-aided design (CAD) software or medical imaging techniques (e.g., computer tomography and magnetic resonance), the latter allowing the generation of patient-specific implants. The model is subsequently tessellated as an STL file that represents the 3D model by a number of three-sided planar facets (triangles), each facet defining part of the external surface of the object. Finally, the STL model is mathematically sliced (SLI model) into thin layers (typically 25–100 μm thick) by using either uniform slicing (where layer thickness is constant throughout the model) or adaptive slicing (where layer thickness changes according to the model surface geometry) model methods [1, 19, 81].

Photo-fabrication technologies are currently used for several applications, such as ① generating 3D structures by inducing the establishment of crosslinks between prepolymers in solution (“additive mode”), ② promoting the local cleavage of photosensitive moieties, leading to a spatiotemporally controlled disruption of the polymer network (“subtractive mode”), ③ assisting the 3D printing of bioinks (“additive mode”), or ④ mediating the patterning of biomolecules (“additive mode”). In the following sections, we describe the principles of the photo-fabrication techniques and strategies that are used to engineer 3D constructs for tissue engineering and drug delivery applications.

### 3.1 Single- and two-photon stereolithography

Stereolithography is an additive biofabrication technique that produces 3D solid objects in a layer-by-layer procedure through the selective photo-initiated curing reaction of a liquid photosensitive material. The curing reaction is triggered by the incidence of light with an appropriate wavelength (UV, visible, or near-infrared [near-IR]), intensity, and duration, resulting in two distinctive processes: single-photon polymerization or two-photon polymerization. Although the chemical principle of these processes is similar, single-photon polymerization involves the absorption of a sole photon, while in 2PP, the molecule simultaneously absorbs two photons with relatively low intensity, and is excited to a higher singlet state. As the probability of the electronic excitation of a molecule by simultaneous absorption of two photons depends quadratically on the incident light intensity, 2PP allows a submicron 3D resolution (~200 nm) with greater depth and ultrafast fabrication [45, 81].

Stereolithographic processes produce 3D structures in a layer-by-layer fashion using two fundamental irradiation approaches: ① direct or laser writing and ② mask-based writing (Figure 4). The first employs a focused laser beam to selectively induce the polymerization of a liquid photopolymer, while the second transfers an entire image to a liquid prepolymer by irradiating through a patterned mask that contains transparent zones corresponding to the sections of the model to be built. The major advantage of the mask-based approach lies in the fast processing and the low-density flux of light over the prepolymer, which avoid undesirable polymerizations [81, 82].

Traditional stereolithography apparatus consists of a vat loaded with prepolymer, a computer-controlled platform in which the model is built, a light source,

and a system that projects light over the prepolymer. In the laser-writing approach, a computer-controlled dynamic mirror system guides and projects the laser beam in a point-by-point scanning manner over the photosensitive prepolymer. In contrast, in the mask-based approach, liquid crystal display panels and digital micromirror devices (DMDs) are used to quickly generate the masks with precise alignment to illuminate a pattern on the prepolymer surface. Once one layer is solidified, the platform dips into the polymer vat and the cured layer is recoated with a uniform layer of the liquid prepolymer for subsequent irradiation. The process is sequentially repeated until the 3D structure is complete. Post-processing steps are usually required to remove the non-polymerized prepolymer and, for some applications, to promote the post-curing of the structure [81, 82].

Although conventional stereolithography has superior resolution and accuracy to other additive biomanufacturing techniques (e.g., melt extrusion or inkjet printing), advances in engineering and photonics have led to the development of alternative processes with higher resolution, such as microstereolithography and 2PP stereolithography. In microstereolithography, the laser beam is more precisely focused, which reduces the spot size to a few micrometers in diameter, improving the resolution of the process. For example, in DMD-based microstereolithography, the achievable lateral and vertical resolutions are ~2 μm and ~1 μm, respectively [83]. To date, 2PP stereolithography is the most advanced technique, allowing the ultra-fast fabrication of constructs with 3D submicron resolution (> 65 nm) by using a focused femtosecond near-IR (~800 nm) wavelength to induce polymerization [84]. In 2PP, the polymerization can occur under the material surface, but it is limited to the focal point of the femtosecond laser, due to the strong decrease in the number of excited molecules as the distance from this region increases. As a result, 2PP stereolithography allows for a fine control over polymerization in a 3D environment [84]. Although this technology possesses numerous advantages, 2PP systems are still very expensive and

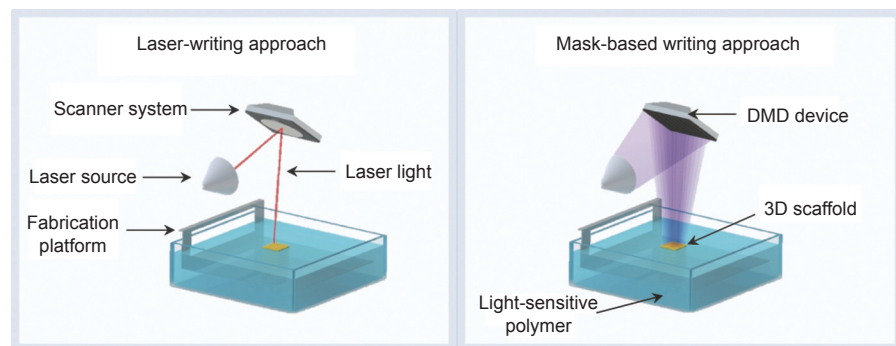


Figure 4. Illustration of light irradiation approaches in stereolithography.

operate with a single material, which precludes the fabrication of multi-material constructs [45, 79]. To circumvent these limitations, Bártolo and coworkers developed a mask-based multi-photon and multi-material stereolithographic system, designated as micro stereo-thermal-lithography ( $\mu$ STLG) [85]. This system can operate in three distinct modes by using UV and near-IR radiation effects, alone or simultaneously, to generate free radicals for polymerization (Figure 5). Rather than processing one material at a time, the  $\mu$ STLG apparatus includes a multi-vat system that enables the fabrication of multi-material constructs [79, 86, 87]. Projection-based stereolithography represents another useful variant of traditional stereolithography, in which 2D patterns generated by DMDs are projected over the liquid resin through a transparent, non-adhering plate. In this setup, the support platform dips into the resin, and the structure is not exposed to oxygen during light irradiation, significantly reducing the oxygen inhibition [81, 88]. Recently, Tumbleston et al. [89] developed a new variation of traditional stereolithography that allows the rapid (minutes instead of hours) and continuous fabrication of 3D structures with resolution below 100  $\mu$ m. In this process, termed as continuous liquid interface production (CLIP), a continuous sequence of images generated by a UV digital light-processing imaging unit is projected through a UV-transparent and oxygen-permeable build window, above which the object is built. The oxygen-permeable window permits the formation of an oxygen-containing “dead zone,” that is, a thin uncured liquid layer, between the build window and the surface of the crosslinked structure. The thickness of the thin uncured liquid layer (in the range of tens of micrometers) can be adjusted by optimizing the operating parameters, preventing the adhesion of the structure to the transparent window, and allowing the continuous drawing out of the object from the vat during the fabrication. The elevation of the object from the resin vat generates suction forces that continuously renew the photosensitive polymer in the surface of the structure, precluding intermediate, time-consuming re-coating and re-positioning operations. Since the slicing

thickness does not affect the fabrication speed, the CLIP process allows the rapid fabrication of smooth structures without increasing the fabrication time, which is impossible in conventional stereolithography. The resolution and rapid fabrication of the CLIP process make it very attractive for engineering complex constructs with clinically relevant dimensions, and intricate architectures for biomedical applications.

### 3.1.1 Stereolithography for scaffold-based therapies

The fabrication of 3D scaffolds with intricate microarchitectures is one of the most explored applications of stereolithography in the biomedical field. In scaffold-based therapies, stereolithographic processes are applied to produce scaffolds that can be directly implanted into the lesion, or seeded with cells for later implantation. As the prepolymer solution contains neither living cells nor therapeutic molecules, the range of processable biomaterials is not limited to natural and synthetic hydrogels [90–92], but also includes biodegradable thermoplastic polymers, such as propylene fumarate (PPF) [93], poly( $\epsilon$ -caprolactone) (PCL) [94], poly(D,L-lactide) (PDLLA) [95], and poly(trimethylene carbonate) (PTMC) [96]. After modification with light-reactive groups, these prepolymers are usually mixed with reactive (e.g., diethyl fumarate [DEF]) or non-reactive (e.g., propylene carbonate) diluents to reduce the viscosity and provide enhanced control over the degree of crosslinking and the mechanical properties of the scaffolds [81, 96, 97]. Alternatively, solvent-free approaches have also been developed to suppress the use of non-degradable diluents in order to allow the fabrication of constructs with enhanced biodegradability and biocompatibility [90, 95]. A residual amount of Orasol Orange dye is commonly added to the resin formulation in order to precisely control the penetration depth of the light into the liquid prepolymer [96, 98].

Most of the studies involving the stereolithography of acellular scaffolds are devoted to assessing the applicability and cytotoxicity of the developed resins, rather than demonstrating their efficacy *in vivo* [90, 93, 95, 97, 99, 100]. In one example, Leigh et al. [90] developed a series of inhibitor- and solvent-

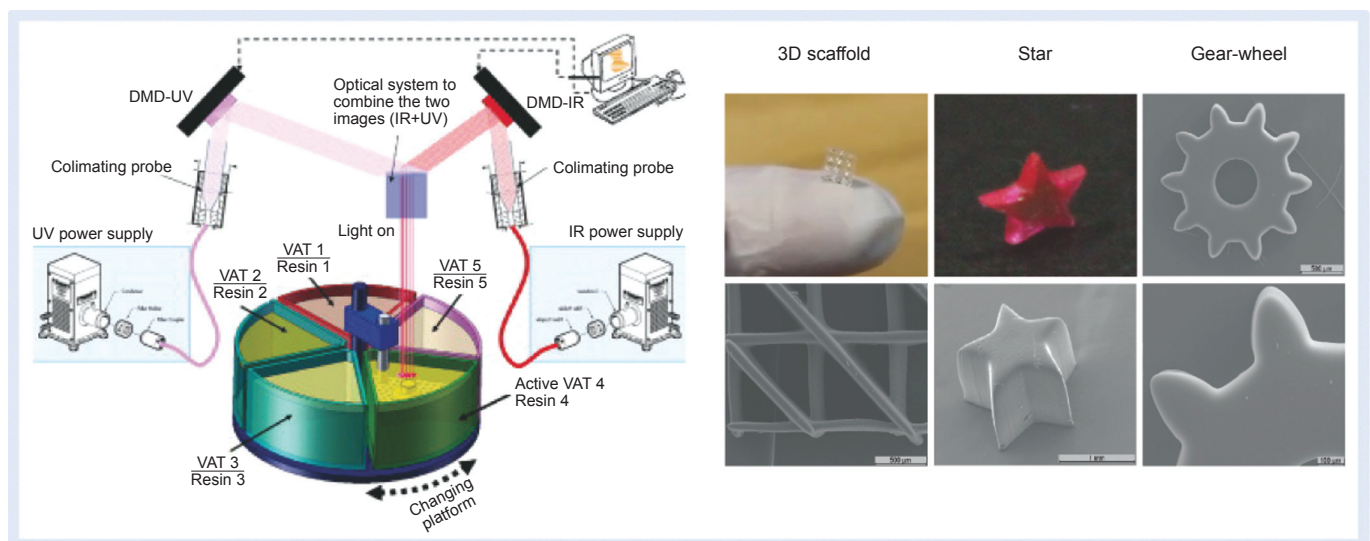


Figure 5. Micro stereo-thermal-lithography system and examples of produced 3D structures.

free PEG-based resins, and demonstrated their processing into porous 3D scaffolds using a microstereolithography device. After 1 week of culture, the scaffolds supported the adhesion and proliferation of human bone-marrow-derived MSCs. In a similar work, flexible and elastic scaffolds based on three-armed methacrylated PTMC resins were prepared by stereolithography for cartilage tissue engineering applications [96]. Bovine chondrocytes covered the scaffold surfaces and secreted sulfated glycosaminoglycans and fibrillar collagens during 6 weeks of culture, leading to a significant increase in the compressive modulus of the constructs. More recently, Gonçalves et al. [101] synthesized a series of biobased unsaturated polyesters through the bulk polycondensation of biobased aliphatic diacids (succinic, adipic, and sebacic acid) and two different glycols (propylene glycol and diethylene glycol), using fumaric acid as a photoreactive group. Cyto-compatible resin formulations were successfully processed in 3D scaffolds using the  $\mu$ STLG system.

Although these works demonstrate the ability of 3D scaffolds to support cell functions, the lack of biological functionality in synthetic polymer networks is still an important limitation on optimal cell guidance and new tissue formation. To address these issues, the surfaces of 3D scaffolds can be treated with cell-adhesive peptides or calcium-phosphate-based coatings to improve cell adhesion and integration into the host tissue [102, 103]. A recent study showed that the surface modification of porous PPF scaffolds with calcium-phosphate-based coatings combined with the delivery of recombinant human bone morphogenetic protein-2 (rhBMP-2) is an effective approach to promote *in vivo* bone healing [102]. Using a different strategy, Elomaa et al. [104] explored the copolymerization of  $\epsilon$ -caprolactone and L-alanine-derived depsipeptide in order to tailor the properties of synthetic polymers. The incorporation of depsipeptide increased the hydrophilicity, hydrolytic degradation, and compressive strength of 3D scaffolds, without compromising the viability, proliferation, and differentiation of cells seeded in photocrosslinked films. One alternative strategy to overcome the limited cell-interactive properties of synthetic polymers and to avoid time-consuming, expensive surface-modification pathways consists of engineering photopolymerizable natural polymers for stereolithography. Gauvin et al. [105] demonstrated the feasibility of mask-based stereolithography to produce complex porous scaffolds based on gelatin methacrylate, which naturally contains cell adhesion sites and degradable moieties. Dynamically seeded human umbilical vein endothelial cells (HUVECs) adhered and proliferated on the scaffolds, maintaining the characteristic phenotype.

For applications in load-bearing tissues with heterogeneous composition, such as bone, thermoplastic polymers are usually reinforced with ceramic-like materials. These formulations not only combine the best properties of each material, but more importantly enable the fabrication of scaffolds that mimic the organic and non-organic phases of bone tissue. Particular attention has been paid to the influence of ceramic particles on the viscosity of prepolymers and the bioactivity of 3D scaffolds [106–108]. For example, bioactive glass S53P4 and methacrylated PCL prepolymer were combined to pro-

duce 3D scaffolds with gyroid pore network architecture. Bioactive glass was homogeneously dispersed throughout the scaffold, allowing the formation of calcium phosphate deposits on the scaffold surface, and stimulating the proliferation of fibroblasts [107]. Alternative biofabrication strategies have also been reported in producing ceramic scaffolds through stereolithography. In general, these strategies involve the polymerization of a polymer/ceramic slurry, followed by the removal of the polymer (via thermal or dissolution treatment), and the sintering of ceramic particles [88].

2PP stereolithography is an attractive technique to produce 3D scaffolds with enhanced resolution, using natural and synthetic polymers [92, 109–112]. Kufelt et al. [110] explored the use of 2PP stereolithography to produce 3D scaffolds based on hyaluronic acid and PEG diacrylate. To demonstrate the potential of this formulation for the delivery of relevant factors, they conjugated epidermal growth factor (EGF) to the functionalized hyaluronic acid, and assessed the effects of EGF release on cell density. In a similar work, gelatin was chemically modified with methacrylamide side groups, and subsequently processed into 3D scaffolds capable of promoting the adhesion, proliferation, and differentiation of mesenchymal stem cells [92]. Despite growing interest in 2PP stereolithography, the number of suitable prepolymers and two-photon photoinitiators is still a major limitation of this technology [84].

In one of the few examples demonstrating the capability of stereolithography to engineer 3D scaffolds for the delivery of growth factors, Lee et al. [16] employed a microstereolithography system to polymerize a resin formulation composed of PPF/DEF photopolymer and BMP-2-loaded poly(lactide-co-glycolic acid) (PLGA) microspheres. To assess the *in vivo* bone formation, BMP-2-loaded scaffolds produced by either microstereolithography or particulate leaching/gas foaming (a conventional scaffold for comparison) were implanted into a rat cranial defect. After 11 weeks of implantation, results showed a significant increase in new bone formation on the defects treated with the scaffold produced by microstereolithography, which reveals the positive effect of growth-factor release and the influence of biofabrication techniques on bone healing (Figure 6). Later, the same research group reported the superior performance of PPF scaffolds containing BMP-2-loaded PLGA microspheres, and seeded with human adipose-derived stem cells, for promoting *in vivo* bone formation in rat crania over acellular scaffolds [113]. In another study, porous 3D PPF scaffolds were coated with both rhBMP-2 (at different doses in collagen) and calcium phosphates, and their ability to promote *in vivo* bone regeneration was evaluated over 6 weeks in a bone-defect rabbit calvarial model [101]. Results showed that the synergetic effect between rhBMP-2 release and calcium phosphate coatings (in particular magnesium-substituted  $\beta$ -tricalcium phosphate and carbonated hydroxyapatite) promoted the new bone formation. Stereolithography was also applied to create biodegradable PTMC networks for drug delivery applications [114]. Fumaric acid monoethyl ester-functionalized PTMC oligomers were copolymerized with hydrophilic *N*-vinyl pyrrolidone (NVP) and hydrophobic vinyl acetate (VAc) at dif-

ferent ratios in order to obtain networks exhibiting different ranges of hydrophilicity. PTMC networks were loaded with vitamin B12 as a model drug, and crosslinked by exposure to UV light. *In vitro* release studies showed that PTMC networks allow the sustained release of vitamin B12 during 23 weeks, while the release kinetics can be controlled by changing both the hydrophilicity and the crosslinking density of polymer networks.

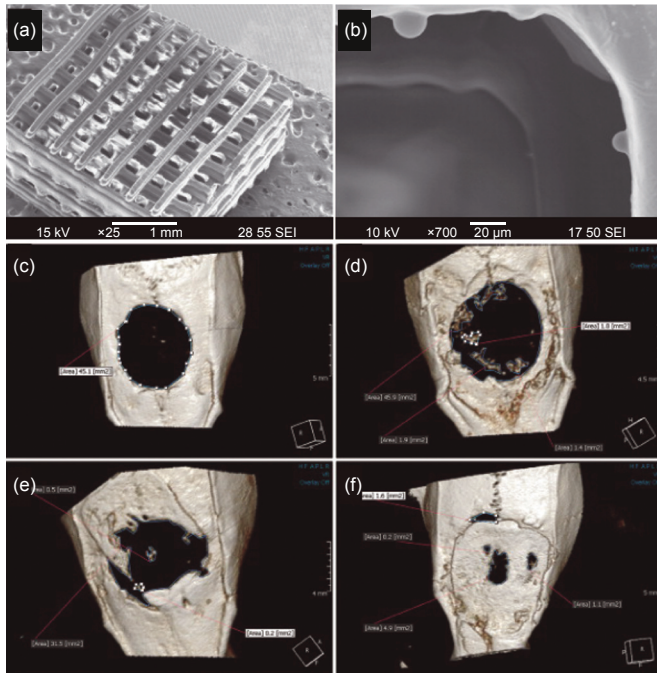


**Figure 6.** (a) SEM images of BMP-2-loaded PPF scaffold produced by microstereolithography; (b) showing the embedded PLGA microspheres; (c) Micro-CT images of bone regeneration after 11 weeks of implantation: negative control; (d) BMP-2-unloaded conventional scaffold; (e) BMP-2-unloaded microstereolithography scaffold; (f) BMP-2-loaded microstereolithography scaffold [16].

Due to its unique resolution and ability to create small-scale devices, stereolithography has also been widely explored to fabricate microneedles for the delivery of drugs into and through the skin. Gittard et al. [115] combined 2PP stereolithography and polydimethylsiloxane (PDMS) micromolding technologies to fabricate microneedle arrays from a photosensitive polymer system composed of poly(ethylene glycol) 600 diacrylate, gentamicin sulfate, and Irgacure 369 as the photoinitiator. 2PP stereolithography was used to create solid microneedle arrays, which were subsequently applied to generate negative molds through PDMS micromolding. Then the PDMS molds were used to obtain microneedle arrays by molding and curing the photosensitive polymer system. Microneedles with base diameters of 150  $\mu\text{m}$ , lengths of 500  $\mu\text{m}$ , tip angles of 45°, and >10  $\mu\text{m}$  tip diameters were successfully obtained by the stereolithography-micromolding method. Agar plating assay showed that gentamicin was released from the microneedles, inhibiting the growth of *Staphylococcus aureus* bacteria. In another work, visible-light dynamic-mask microstereolithography and pulsed laser deposition were combined to produce antimicrobial microneedles for the local treatment of skin infections. Microstereolithography

was explored to create microneedles using a photosensitive acrylate polymer (eShell 200), which were then coated with silver or zinc oxide thin films using pulsed laser deposition. Microneedles penetrated into porcine skin, exhibiting remarkable antimicrobial activity against *Staphylococcus epidermidis* and *Staphylococcus aureus* [116].

### 3.1.2 Stereolithography of cell-laden hydrogels

A distinctive feature of stereolithographic processes is their ability to process living cells and sensitive molecules embedded in hydrogel precursors under biocompatible conditions with high resolution and accuracy. These capabilities have been explored as a way to engineer complex 3D microenvironments *in vitro* that resemble the structural and compositional characteristics of the natural ECM. Such environments are fabricated by the selective photopolymerization of cell-laden hydrogel precursors, and play a key role in the study of cell response to biochemical cues and the elucidation of mechanisms underlying cell-cell and cell-material interactions [117, 118]. The direct fabrication of 3D poly(ethylene glycol) diacrylate (PEGDA) constructs with RGDS (Arg-Gly-Asp-Ser) functionalization and embedded NIH/3T3 fibroblasts was realized in a modified stereolithography system by exploring both top-down and bottom-up approaches. Although 2 mm thick constructs were produced through a top-down approach without impairing cell viability, a heterogeneous distribution of cells was observed as a result of cell settling on the bottom of the reservoir. In contrast, the bottom-up approach allowed the fabrication of constructs with homogeneous cell distribution, although this approach involved the manual delivery of cells. Using the latter approach, Chan et al. demonstrated the feasibility of their strategy to engineer multilayer 3D constructs with labeled cells placed in pre-designed spatial locations, as shown in Figure 7(a) [119]. A similar strategy was recently explored by the same research group to create complex 3D constructs containing multiple cell types encapsulated within hydrogels at specific locations, for the purpose of studying reciprocal interactions between two cell types (Figure 7(b)). Results clearly showed that factors secreted by skeletal muscle myoblast cells enhanced the neuronal functionality of primary hippocampus neurons (a 2.5 times increase) through co-encapsulation, which proves the usefulness of stereolithography for such applications [118]. In another study, a projection stereolithography system emitting visible light was employed to fabricate 3D hydrogel scaffolds using human adipose-derived stem cells suspended in PEGDA, with LAP as the photoinitiator, and Percoll to prevent cell settling. Cells encapsulated within porous 3D scaffolds remained viable (> 90%) throughout the construct for 7 days post-fabrication [120]. Recently, 2PP stereolithography was explored for the first time to generate 3D constructs in the presence of living cells. An initial screening was first carried out to assess appropriate 2PP photoinitiators, followed by the suspension of human osteosarcoma cells in methacrylamide-modified gelatin and subsequent photopolymerization. Findings revealed that reactive species produced during 2PP might be the cause of the observed cell damage, since the operating parameters do not impair the viability of cells.

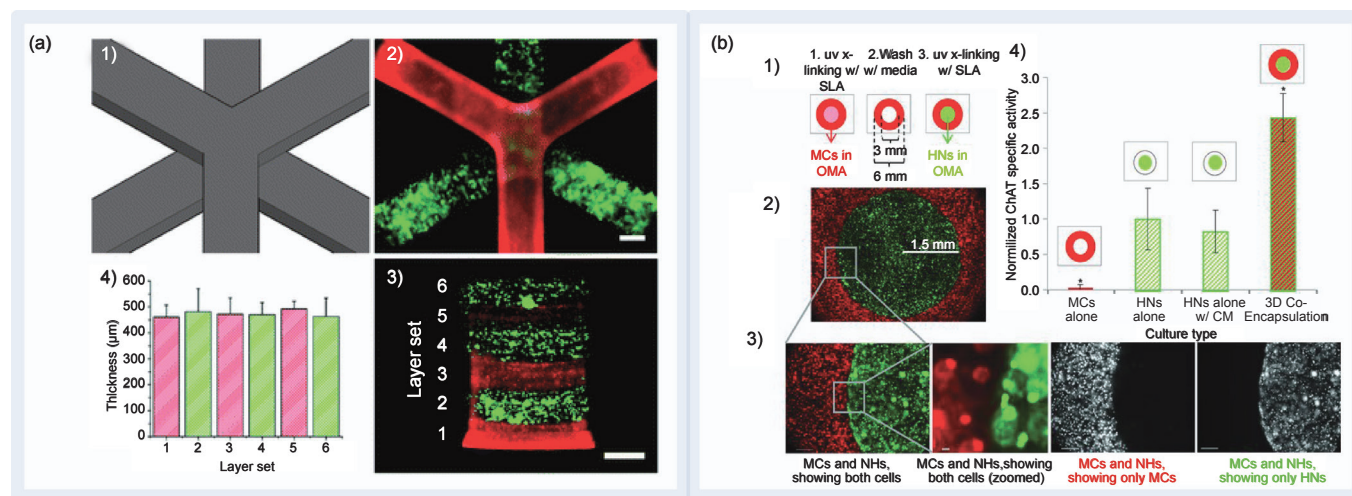


**Figure 7. Cell-laden hydrogel constructs produced by stereolithography.** (a) 3D hydrogels fabricated by the layer-by-layer irradiation of PEGDA prepolymer containing fibroblast cells, exhibiting uniform layer thickness (scale bars represent 1 mm) [119]; (b) fabrication of co-culture environments of skeletal muscle myoblast cells and primary hippocampus neurons to assess the effects of proximity between cells on the functionality of the neurons quantified by measuring their choline acetyltransferase (ChAT) activity after 10 days of culture [118].

Cells encapsulated within the matrices and cultured for 3 weeks were able to proliferate and migrate to the empty spaces within the construct [121].

### 3.2 Laser direct-write techniques: 3D printing of cells through light-mediated effects

Laser direct-write techniques employ light energy to precisely print biomaterials, cells, and therapeutic molecules onto a receiving substrate. Although the purpose of these techniques is not to trigger photopolymerization reactions, they can be coupled to stereolithographic processes in order to engineer complex constructs that have cells placed in specific 3D locations within photocrosslinked gels [122]. Laser direct-write techniques afford the fabrication of complex 3D environments with high resolution and accuracy in a multi-layered printing procedure by using computer-controlled substrates. Since the resolution provided by these processes cannot be achieved by other bioprinting techniques, they are very attractive for the engineering of ECM-like environments.

#### 3.2.1 Laser-guided direct writing (LGDW)

Laser-guided direct writing (LGDW) is an orifice-based biofabrication technique that uses optical forces from the scattering of energetic photons in a weakly focused continuous near-IR laser to directly propel cells onto receiving surfaces (e.g., collagen or matri-

gel) with micrometer resolution. The incident photons are focused through a low-numeric-aperture lens, generating radiation forces that trap and guide cells onto the target based on the differences in the refractive index between the cells and the surrounding medium (Figure 8) [123]. LGDW apparatus consists of a weakly focused beam, a suspension containing the cells, a receiving substrate, and a computer-controlled moveable system to control the cell deposition [124]. A conventional system affords the guidance of cells over a distance of ~300 μm due to the laser beam divergence and convective fluid flow forces. In more advanced apparatus, the inclusion of a hollow optical fiber allows cell transport over distances up to 7 mm with increased quality of deposition [125]. LGDW has been used to print several cell types in 2D and, to a limited extent, 3D patterns without compromising the cell viability [123, 125, 126]. Although LGDW was a pioneer technology in patterning living cells, its low cell throughput (2.5 cells·min<sup>-1</sup>) and poor reproducibility, along with the development of more effective techniques, have significantly limited its usage in tissue engineering [124].

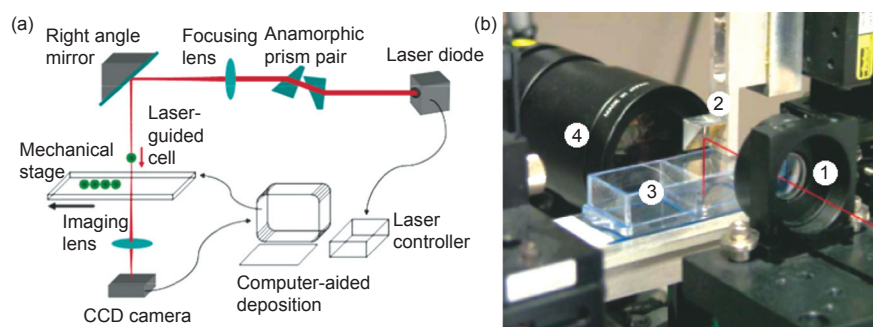


**Figure 8. Typical apparatus of a LGDW system.** (1) Focusing lens; (2) right-angle mirror; (3) sealed glass chamber-slide; and (4) optional side-on imaging lens [123].

#### 3.2.2 Laser-induced forward transfer (LIFT)

Techniques based on laser-induced forward transfer (LIFT) make use of a high-energy pulsed laser to induce local melting of a liquid suspension, leading to its ejection towards a receiving substrate. In contrast to LGDW, the orifice-free nature of LIFT-based processes precludes issues related to clogging, viscosity, and contamination; however, specific conditions must be satisfied in order to achieve droplet formation and ejection. The droplet formation mainly depends on laser and bioink properties (e.g., laser fluency, bioink viscosity, and film thickness) and includes three distinct modes: sub-threshold (no material deposition), jetting (well-defined

jet formation), and plume (formation of atomized droplets) [127].

Conventional LIFT was originally applied in the direct writing of metals, but its unique resolution and patterning capabilities have also been explored for biomedical applications by introducing several modifications to the traditional apparatus. For example, modifications were done on the laser source and the composition of printing ribbon in order to prevent damage to biological materials and to improve the printing reproducibility. Potential deleterious effects to cells during printing can also be significantly reduced, or even eliminated, by carrying out a careful optimization of the processing parameters, such as the laser pulse characteristics, viscosity of the bioink, thickness of the absorbing layer, and substrate properties [128–130]. Modified-LIFT techniques for biofabrication can be classified into two categories, according to the composition of the print ribbon: matrix-assisted pulsed laser evaporation direct writing (MAPLE DW) and biological laser processing (BioLP). Despite minor differences, the common setup for both techniques consists of a pulsed laser source, a donor slide or print ribbon from which the biological material is printed, and a collector substrate located a few hundred micrometers from the donor slide that receives the printed droplets [124].

MAPLE DW uses a low-powered, pulsed laser operating in the UV or near-UV wavelength (typically 193 nm) that is focused by a microscope objective at the interface between the print ribbon and the optical absorbing material, resulting in local heating, vaporization of the biopolymer layer, and ejection of the cell suspension (Figure 9). The print ribbon is a laser-transparent quartz disk that is coated with a sacrificial biopolymer layer, which contains the cells [131]. The biopolymer layer, usually composed of gelatin, or Matrigel, provides initial cell attachment, absorbs the incident laser light, and promotes the energy transfer to generate the droplet ejection. However, this layer does not eliminate the interaction between the incident light and the cell suspension. MAPLE DW can achieve a spatial resolution of less than 10 mm [131].

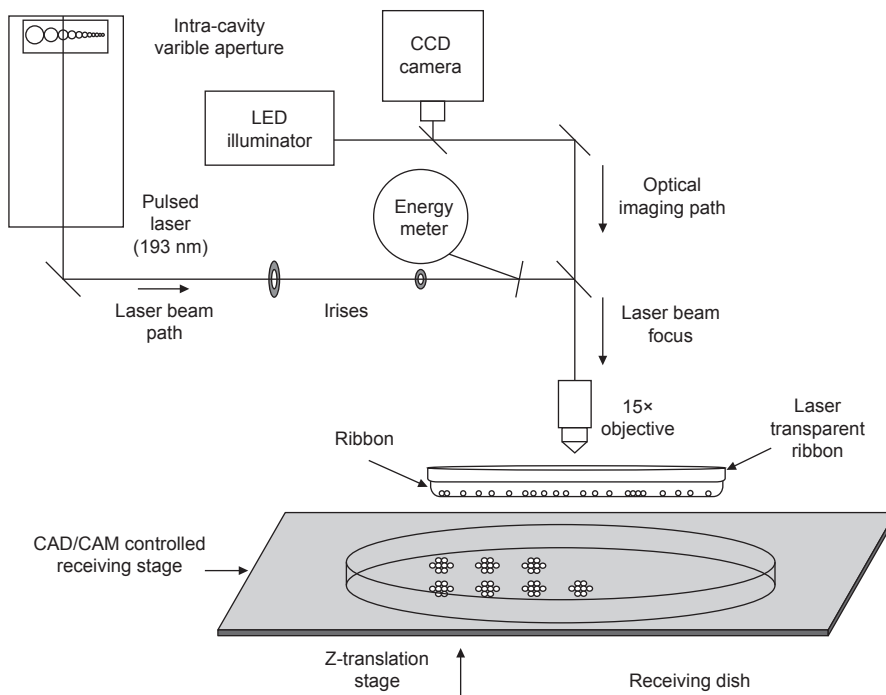


**Figure 9. Schematic illustration of the MAPLE DW apparatus.** (Adapted from Ref. [132])

The capability of MAPLE DW to pattern mammalian cells into arbitrary substrates in an organized manner while exhibiting high post-printing viability was demonstrated by several research groups [133–136]. Schiele et al. [135] developed a novel strategy to print viable cells involving the use of gelatin to coat the print ribbon and the receiving substrate; in this way, they avoided the presence of factors

that might interfere with the cell fate. Human dermal fibroblasts were printed through this strategy, and exhibited high viability and an absence of DNA damage. This strategy was further explored in order to recreate a stem cell niche by precisely patterning embryonic stem cells onto a gelatin-coated substrate. Printed cells remained viable (~87%) and undifferentiated upon deposition, forming embryoid bodies after 7 days in culture. Furthermore, the differentiation ability of embryonic stem cells was not compromised by the printing process [132]. MAPLE DW was also explored for the co-patterning of MG 63 osteoblast-like cells in the presence of hydroxyapatite, demonstrating the possibility of printing composite bioinks [137].

Biological laser processing (BioLP), also referred as laser-assisted bio-printing (LaBP), represents the most advanced laser-assisted technique currently available. In this technique, a biocompatible laser-absorption inter-layer (1–100 nm) is included between the print ribbon and the cellular layer (Figure 10), providing numerous advantages over its MAPLE DW counterpart: ① eliminating interaction between the laser and the biological material, ② reducing heating, ③ allowing more efficient droplet ejection, and ④ providing superior reproducibility [80, 127]. Droplet formation and ejection is achieved by focusing a high-powered laser pulse (usually a near-IR laser) onto the absorption layer, generating local heating and vaporization with consequent vapor bubble formation and expansion [127].

In the context of tissue engineering, BioLP has been explored to fabricate cell-laden constructs for tissue regeneration and 3D environments to elucidate interactions between cells and biomaterials [33, 139–141]. A good demonstration of the capabilities of BioLP to engineer complex, organized cell-laden matrices for tissue regeneration was realized by the fabrication of bilayered 3D skin substitutes. In this study, fibroblasts and keratinocytes were separately embedded in collagen, and subsequently printed onto a slide coated with Matrigel. After 10 days of culture, the constructs maintained

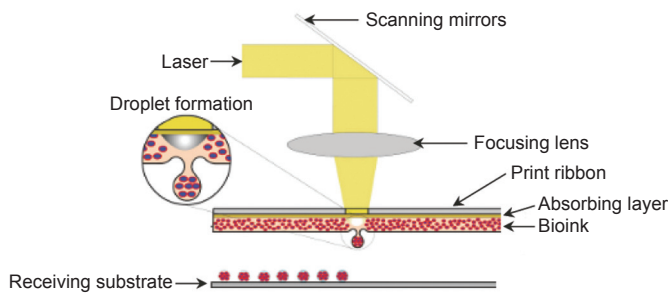


Figure 10. BioLP apparatus. (Adapted from Ref. [138])

the structural organization, and functional cell-cell junctions were detected between the cells [140]. The resolution and multi-cell printing capabilities of BioLP were also explored in an attempt to mimic vascular networks through the printing of branch/stem structures of human umbilical vein endothelial cells (HUVEC) and human umbilical vein smooth muscle cells (HUVSMC) [141]. In addition to the printing of cells embedded in polymers, BioLP enables the patterning of composite bioinks made of biopolymers, cells, and ceramics, opening promising perspectives for applications in the tissue engineering of mineralized tissues. Guillemot et al. [33] demonstrated the printing of human endothelial cells suspended in sodium alginate and nano-sized hydroxyapatite. Droplets with diameters of 70  $\mu\text{m}$  and containing 5–7 cells per drop were patterned onto a quartz disk, and cells remained viable for up to 11 days post-printing. Recently, the same research group reported the sequential printing and assembly of nano-sized hydroxyapatite and human osteoprogenitor cells for engineering 2D and 3D constructs [138]. In a combinatorial biofabrication strategy, the unique resolution of BioLP was explored in order to pattern multiple cells in specific spatial locations of PEGDA hydrogels that were produced by 2PP stereolithography. 3D cellular constructs were fabricated by precisely seeding vascular smooth-muscle-like cells into the outer scaffold area, and endothelial cells into the inner scaffold area, demonstrating the advantages of integrating photofabrication techniques [122].

Although most of the available studies involving BioLP are focused on the printing parameters and their influence on cell fate *in vitro*, it was possible to identify impressive works dealing with the *in vivo* evaluation of 3D cell-laden matrices for skin tissue engineering and the *in vivo* biofabrication of implants for bone healing. In the first case, 3D skin substi-

tutes containing fibroblasts and keratinocytes arranged in two separate regions were implanted in full-thickness skin wounds created in nude mice. Results indicated the formation of a thin stratified tissue in the epidermal region and the presence of new collagen secreted by fibroblasts, evidencing the formation of new skin-like tissue [142]. In the second case, BioLP was employed to print nano-hydroxyapatite directly onto a mouse calvaria defect model *in vivo* (Figure 11). Despite the heterogeneity of the results, it was possible to implement a biofabrication strategy that allowed, to some extent, the formation of new bone *in vivo*, as indicated by the analysis of decalcified histological sections and micro-computed tomography data [143]. In fact, BioLP is one of the few additive biofabrication techniques that is already employed to produce implants *in vivo*, which represents a great advance toward clinical translation.

### 3.3 Photodegradation and photopatterning reactions: Moving to *in situ* engineering of dynamic 3D microenvironments

Biofabrication strategies, based on photopatterning and photodegradation approaches, are assuming a pivotal role in tissue engineering and cell biology, as they provide spatio-temporal control over the grafting/cleavage of biochemical entities in a 3D environment, without altering neighboring structures. Most importantly, these technologies enable dynamic changes in 3D environments, with submicron resolution at micro- and nano-scales, opening new opportunities for engineering synthetic niches that resemble natural ECM. When contrasted with traditional synthetic environments, natural ECMs are complex and dynamic milieus that provide specific spatiotemporal cues to the cells, determining cell functions such as adhesion, proliferation, differentiation, and morphogenesis. In a similar way, cells sense such biochemical and biomechanical cues via surface receptors, and respond in a dynamic manner through ECM remodeling [28, 61]. Accordingly, our ability to recreate this complex and interactive 3D environment in the laboratory is essential for the development of more effective therapies for tissue repair and regeneration.

3D photopatterning is an exciting strategy for the engineering of dynamic ECM-like environments by using laser or lamp light irradiation to promote the controlled addition of multiple biological entities, either inside or at the surface of a substrate (e.g., hydrogels and nanofibers), with spatial and temporal control. These techniques afford the engineering

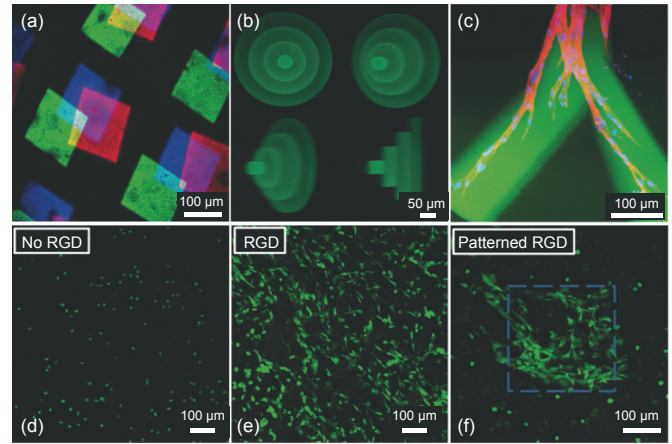


Figure 11. *In vivo* bioprinting using a BioLP system. (a) Illustration of operating setup; (b) mice placed in a specific holder; (c) the bioprinting process. (Adapted from Refs. [143, 144])

of biomimetic constructs containing multiple cells in specific 3D locations, and simultaneously regulate the presentation of biochemical and/or biomechanical cues that influence cell functions in real time and in three dimensions [27, 28, 55, 145–147]. In a typical setup, a cytocompatible photoinitiator and the target molecule are incubated in the presence of the hydrogel, to allow their diffusion inside the polymer network. The desired pattern is then created by irradiating the swelled hydrogel at specific regions, resulting in the anchorage of the desired molecules to the unconsumed photoreactive moieties that were originally introduced in the hydrogel precursor. Light energy from 2PP irradiation is usually preferred, owing to its very small focal volume, fabrication depth, and biocompatibility with biological tissues.

DeForest et al. [27] employed 3D photopatterning to introduce biochemical functionalities within cellular hydrogels that were obtained by reacting a four-arm PEG tetra-azide with bis(DIFO3) di-functionalized polypeptide in the presence of fibroblasts, through a copper-free click chemistry. Upon hydrogel formation, orthogonal thiol-ene photocoupling chemistry was used to pattern peptides at specific locations within the hydrogels, by the establishment of covalent bonds with the photoreactive allyl ester incorporated into the crosslinking peptide. The exact location where the photocoupling reaction occurred was easily controlled, by selectively exposing specific regions within the hydrogel to incident light irradiation, either single or 2PP. The authors showed that their approach allows the facile patterning of a cysteine-containing fluorescently labeled RGD (Arg-Gly-Asp) amino acid sequence within the gels, which locally influences cell attachment and migration (Figure 12). A similar strategy was recently used by Wylie et al. [145] to engineer 3D biomimetic hydrogels with spatial control over the presentation of growth factors (sonic hedgehog and ciliary neurotrophic factors) to stem cells, in order to spatially guide cell fate. This work and others also indicate the ability of 3D photopatterning to realize concentration gradients of proteins that influence cell migration, highlighting the possibility of recreating the gradients of signaling molecules in natural ECMs [145, 148]. In a different approach, Mosiewicz et al. [28] explored the spatiotemporal control conferred by light energy to locally promote the photoactivation of enzyme-mediated bioconjugation reactions, toward the selective tethering of biomolecules. The feasibility of this light-activated enzymatic approach regulates the 3D invasion of mesenchymal stem cells in MMP-sensitive PEG hydrogels, through the selective patterning of the fibronectin-derived adhesion peptide RGD, the recombinant fibronectin fragment FN9-10, and platelet-derived growth factor B.

In addition to its use in the coupling of biochemical entities, photopatterning was also exploited to improve the mechanical properties of 3D hydrogels in space and time. Gramlich et al. [55] applied photopatterning to enhance the mechanical properties of hyaluronic acid hydrogels by means of thiol-norbornene chemistry. Hyaluronic acid was first functionalized with norbornene groups, and subsequently reacted with di-thiols to allow hydrogel formation in a way that left unreacted norbornene groups in the polymer backbone upon



**Figure 12. Examples of 3D patterning within hydrogels.** (a) Patterning of fluorescently labeled peptide sequences within a hydrogel using photomasks and a thiol-ene reaction; (b) 3D micrometer-scale spatial patterning using a confocal microscope; (c) confocal microscope image of human dermal fibroblasts migrating within a RGDS-patterned region inside a collagenase-sensitive PEG hydrogel; (d–f) effect of RGD patterning on the attachment of fibroblasts within 3D hydrogels, where (d) has no patterning, (e) has full patterning, and (f) has a confined patterning region. (All images were reproduced from Ref. [27], with the exception of image (c), which was reproduced from Ref. [147])

photocrosslinking. Next, secondary photopolymerization reactions between unreacted groups and a di-thiol crosslinker allowed an over two-fold increase in the compressive moduli as compared to the initial value. The authors also demonstrated the ability of the thiol-norbornene pathway to allow the sequential photopatterning of fluorescent dyes within the gel with precise spatial and temporal control. Recently, Mosiewicz et al. [149] developed an alternative approach based on photo-labile caging groups to improve hydrogel stiffness. In their strategy, photo-labile caging groups are employed to temporarily mask one of the functional groups involved in hydrogel crosslinking. Upon light irradiation, the functional groups are reactivated, leading to the formation of local patterns of increased stiffness. This approach was employed to tailor the matrix stiffness of PEG hydrogels synthesized by Michael-type addition chemistry in the range of 3.3–8.2 kPa, and to assess its effects on the migration of human mesenchymal stem cells. Owing to their versatility, photopatterning technologies have also been employed in other substrates, including the immobilization of vascular endothelial growth factor in 3D scaffolds with a patterning depth of 500  $\mu\text{m}$  [150], and the creation of RGD peptide patterns in nanofibers produced through electrospinning with the purpose of guiding cell behavior [151]. Photopatterning was also applied for the immobilization of growth factors (bFGF and BMP-2) in PCL/gelatin fibrous scaffolds, in order to regulate the osteogenesis of human mesenchymal stem cells (hMSCs) [152]. In this strategy, bFGF was loaded onto the fibers and BMP-2 was immobilized within the PEG hydrogel patterns in order to afford the sequential delivery of low doses of bFGF during the early stages, and the sustained release of BMP-2 over long periods. Cell culture studies showed the positive contribution of controlled and sequential delivery of growth factors on the osteogenic differentiation of hMSCs compared to the individual release of both factors (Figure 13). In another work, thiol-ene chemistry was explored to immobilize thio-



lated transforming growth factor- $\beta$ 1 (TGF- $\beta$ 1) in step-growth PEG hydrogels for the local presentation of the growth factor to embedded chondrocytes [153]. This approach was successfully applied to covalently bound TGF- $\beta$ 1 throughout the hydrogel in a homogenous manner, without altering its bioactivity. Local and sustained delivery of TGF- $\beta$ 1 resulted in increased DNA content, glycosaminoglycan, and collagen secretion by chondrocytes within the hydrogel over 4 weeks, when compared to the cells in the presence of soluble growth factor delivered in the media. Together, results demonstrated the usefulness of light-mediated reactions for tethering and releasing growth factors to enhance cartilage tissue regeneration.

Photodegradation is emerging as a powerful tool to manipulate cell environments in real time by altering hydrogel features in a subtractive manner, rather than through the addition of biological cues or biomaterials. Therefore, these reactions are capable of mimicking, to some extent, some key events of natural tissues, including ECM remodeling and proteolysis during wound healing. Increasing interest in photodegradation for biomedical applications has boosted research on novel photodegradable hydrogels [78, 154–156]. The merits of photodegradation have been explored for a variety of applications, including the manipulation of cell behavior in 3D environments and the control of the release of therapeutics. The basic concept of photodegradation involves the use of localized light irradiation to trigger the photolysis of photosensitive moieties (*o*-nitrobenzylether, biaryl-substituted tetrazole, and coumarin-based moieties), which leads to the spatiotemporal cleavage of polymeric crosslinks and/or to the release of therapeutics [72, 157–159]. In contrast to other degradation mechanisms such as hydrolysis and enzymatic degradation, in light-mediated degradation the extent of photolysis is easily controlled in real time by changing the light intensity, exposure time, and wavelength [158, 160].

One of the most useful applications of photochemistry involves the real-time manipulation of matrix elasticity in order to investigate the effects of dynamic changes in cell response or to direct cell phenotype [155, 161, 162]. Kloxin et al. [161] developed photodegradable PEG-based hydrogels capable of encapsulating living cells and undergoing controlled degradation upon light irradiation. This dynamic system was explored as 2D culture platforms of variable elasticity in order to assess the influence of matrix elasticity ( $\sim$ 32 kPa to  $\sim$ 7 kPa upon 5 min of light irradiation) and gradients of elastic modulus on the fibroblast-myofibroblast differentiation process. Another relevant application of photodegradation involves the localized photocleavage of hydrogel crosslinks in order to guide cell functions in either 3D or 2D environments [32, 71, 160, 163]. This approach was elegantly demonstrated by DeForest and Anseth, who used multiple wavelengths of light to independently control the functionality and architecture of four-arm PEG-based hydrogels produced by a copper-free, strain-promoted azide-alkyne cycloaddition (SPAAC) reaction [160]. The functionality of the hydrogels was tailored by means of thiol-ene photoconjugation reactions in the presence of visible light (490–650 nm for single-photon, 860 nm for 2PP), while the 3D architecture was changed through photocleavage reactions of photodegradable *o*-nitrobenzyl ether moieties upon the exposure of UV light (365 nm for single-photon, 740 nm for 2PP). A thiol-ene photocoupling reaction of peptide ligands and photolysis can be performed in cell-laden 3D hydrogels without cytotoxic effects to the cells ( $>$  95% viability). The authors also showed that these reactions permit spatiotemporal control over the migration of fibroblasts within hydrogels by eroding migration channels in 3D and by decorating their surfaces with a RGD adhesive motif (Figure 14). Recently, Tsang et al. [32] used a similar approach to direct cardiomyocyte organization and alignment in gelatin-based photodegradable hydrogels. Gelatin meth-

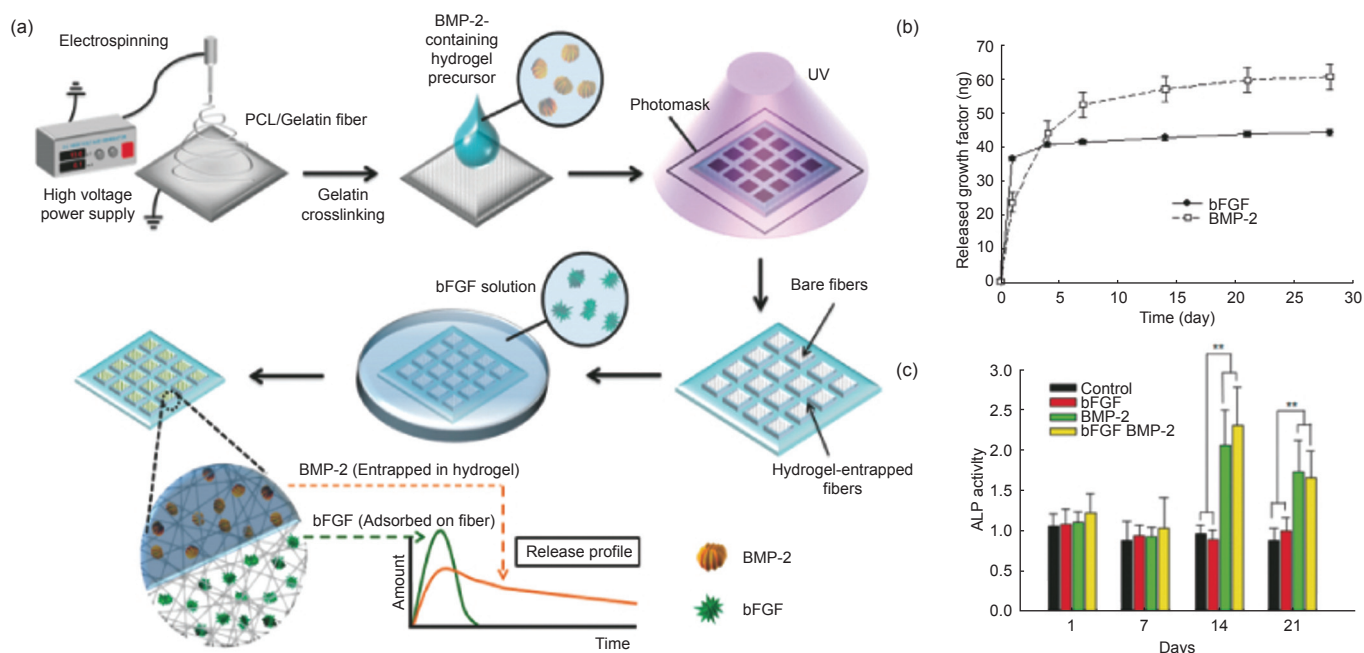


**Figure 13.** (a) Combinatorial biofabrication strategy used to prepare a dual growth factor-loaded scaffold using electrospinning and patterning techniques; (b) in vitro release of growth factors from the scaffolds; (c) their effects on the ALP activity of cultured hMSCs [152].

acrylamide was crosslinked with a photodegradable PEG crosslinker containing both terminal *o*-nitrobenzyl ester and methacrylate moieties to afford photolysis and crosslinking (via redox-initiated polymerization or visible light photopolymerization). Upon exposure to light irradiation (5 min, 320–500 nm, 20 mW·cm<sup>-2</sup>), well-defined microsized patterns were created in the surface of hydrogels in order to control the alignment of seeded neonatal rat cardiac fibroblasts and cardiomyocytes. Photodegradation is also very attractive for the controlled delivery of therapeutics from different vehicles, including nanoparticles, microspheres, and gels [73, 164–169]. In one example, a series of photodegradable polyurethane polymers was synthesized, and exhibited the ability to be assembled into nanoparticles containing encapsulated water-insoluble drugs. In this work, the most promising formulation was loaded with drugs and used for drug delivery studies in the presence of cells. Drug-loaded nanoparticles afford uptake by macrophages and are able to release the drug in the cells upon exposure to external light irradiation [166]. In another work, Azagarsamy and Anseth [73] developed a novel strategy involving the use of two photocleavable units in order to afford the selective and sequential release of multiple proteins (BMP-2, BMP-7) from the same hydrogel. Proteins were covalently conjugated to the hydrogel networks through photocleavable units based on nitrobenzyl ether (photolysis at 365 nm) and coumarin methylester (photolysis at 405 nm), and their temporal release was regulated by varying the wavelength of light, and the intensity and time of light exposure. No modifications on the bioactivity of released proteins were detected through osteogenic differentiation assays involving hMSCs. The spatiotemporal control conferred by light energy was also explored to control the intracellular release of an anti-cancer drug, paclitaxel, inside of human fibroblasts and liver cells [167]. Paclitaxel was loaded in gold nanoparticle-capped mesoporous silica nanospheres (PR-AuNPs-MSN), which were rapidly endocytosed by both cell types. After exposure to UV irradiation (365 nm) for 10 min, a significant decrease in the cell viability was observed for liver (44.2%) and fibroblast (43.5%) cells containing drug-loaded nanospheres. In contrast, PR-AuNPs-MSN without the drug was not cytotoxic for the cells, either before or after UV light irradiation. Collectively, these results highlight the potential of light-mediated reactions for the controlled release of anti-cancer drugs in chemotherapy. In a similar approach, UV light was applied to trigger the delivery of an anti-cancer drug (5-fluorouracil) covalently linked to micelles functionalized with coumarin [poly(ethylene oxide)-*b*-poly(*n*-butylmethacrylate-*co*-4-methyl-7-(methacryloyl)oxyethoxy]-coumarin)] [168]. Micelle-drug conjugates with diameters of 70 nm and exhibiting excellent biocompatibility for L929 cells were obtained through exposure to UV light irradiation of wavelength 350 nm. The release of 5-fluorouracil from the micelle-drug conjugates was achieved by using UV light irradiation of wavelength 254 nm to cleave the photolabile linkers between drug and polymer chains. *In vitro* tests revealed that 68% of the drug was released from the micelle-drug conjugates within 12 h without burst release effect. Although the penetration of UV light into the skin is limited,

thereby precluding the application of micelle-drug conjugates for cancers located in deep tissues, this approach can be translated for light wavelengths with higher skin penetration.

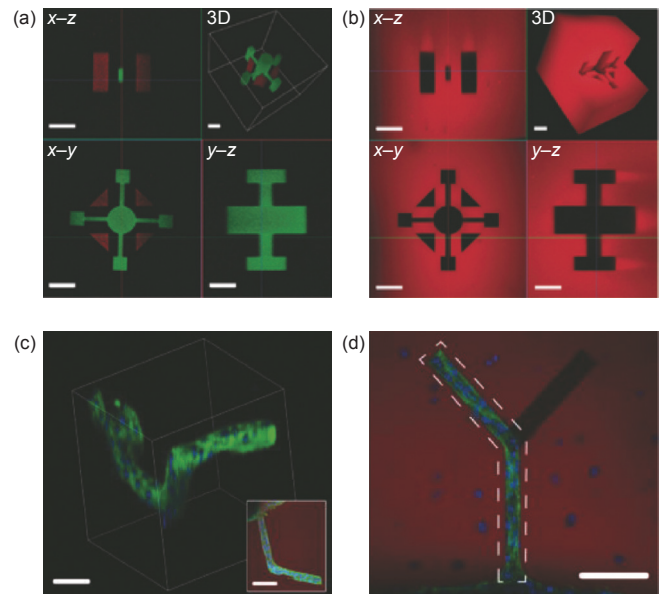


**Figure 14.** (a) Photopatterning of red- and green-labeled patterned peptides within 3D hydrogels using multiphoton laser light ( $\lambda = 860$  nm); (b) 3D photodegradation reaction performed in specific locations with micrometer-scale resolution by using multiphoton laser light ( $\lambda = 740$  nm); (c) manipulation of cell motility within hydrogels containing 3T3-fibroblast-laden clot surrounded by hMSCs cells by combining photodegradation reactions to create channels and photopatterning reactions to decorate the channels with the RGD moiety; (d) cells migrate throughout the construct channels functionalized with RGD [160].

## 4 Concluding remarks

Photo-fabrication technologies are one of the most promising biofabrication strategies for engineering 3D microenvironments for tissue regeneration and the delivery of therapeutics. The multitude of light-mediated reactions currently available permits the fabrication of highly complex matrices with micro- and nano-scale resolution, exhibiting architectural and compositional features that resemble some of the properties of natural ECM. Reactions mediated by light can proceed under biocompatible conditions and in the presence of sensitive compounds such as cells and biochemical signals, allowing the precise positioning of biomaterials and cells in 3D environments. As a result, the fabrication of dynamic 3D constructs containing multiple cell types and decorated with a plethora of biochemical entities such as cell-adhesion motifs, proteolytic domains, and relevant growth factors is now a reality. However, spatiotemporal coordination of the presentation of these factors to the cells at the desired site, concentration, and doses still remains one of the biggest challenges for this technology. In the last decade, these issues have been fully investigated through combinatorial or individual strategies, resulting in significant advances regarding the development of advanced biomaterials, more efficient photochemical reactions (e.g., orthogonal click reactions, photoinitiators, and photoreactive moieties), and biofabrication

technologies with improved resolution. These progresses allowed the *in vivo* 3D printing of bone substitutes through photo-fabrication technologies, which clearly demonstrates the potential of these technologies in the biomedical field. Despite these encouraging advances, systematic *in vivo* studies detailing the effects of newly developed 3D constructs on biological systems, and the interactions of these constructs with biological systems, are still scarce.

## Acknowledgements

The authors thank the support of the Portuguese Foundation for Science and Technology (FCT) through the strategic project UID/Multi/04044/2013. Ruben F. Pereira is grateful to the FCT for the doctoral grant SFRH/BD/91151/2012.

## Compliance with ethics guidelines

Rúben F. Pereira and Paulo J. Bártolo declare that they have no conflict of interest or financial conflicts to disclose.

## References

1. F. P. W. Melchels, M. A. N. Domingos, T. J. Klein, J. Malda, P. J. Bartolo, D. W. Huttmacher. Additive manufacturing of tissues and organs. *Prog. Polym. Sci.*, 2012, 37(8): 1079–1104
2. A. Ranga, M. P. Lutolf. High-throughput approaches for the analysis of extrinsic regulators of stem cell fate. *Curr. Opin. Cell Biol.*, 2012, 24(2): 236–244
3. A. Khademhosseini, R. Langer, J. Borenstein, J. P. Vacanti. Microscale technologies for tissue engineering and biology. *Proc. Natl. Acad. Sci. U.S.A.*, 2006, 103(8): 2480–2487
4. R. S. Tuan, G. Boland, R. Tuli. Adult mesenchymal stem cells and cell-based tissue engineering. *Arthritis Res. Ther.*, 2003, 5(1): 32–45
5. D. J. Newman, G. M. Cragg. Natural products as sources of new drugs over the 30 years from 1981 to 2010. *J. Nat. Prod.*, 2012, 75(3): 311–335
6. P. X. Ma. Biomimetic materials for tissue engineering. *Adv. Drug Deliv. Rev.*, 2008, 60(2): 184–198
7. R. F. Pereira, C. C. Barrias, P. L. Granja, P. J. Bartolo. Advanced biofabrication strategies for skin regeneration and repair. *Nanomedicine (Lond)*, 2013, 8(4): 603–621
8. R. Passier, L. W. van Laake, C. L. Mummery. Stem-cell-based therapy and lessons from the heart. *Nature*, 2008, 453(7193): 322–329
9. R. S. Kirsner, W. A. Marston, R. J. Snyder, T. D. Lee, D. I. Cargill, H. B. Slade. Spray-applied cell therapy with human allogeneic fibroblasts and keratinocytes for the treatment of chronic venous leg ulcers: A phase 2, multicentre, double-blind, randomised, placebo-controlled trial. *Lancet*, 2012, 380(9846): 977–985
10. P. J. Bártolo, C. K. Chua, H. A. Almeida, S. M. Chou, A. S. C. Lim. Biomanufacturing for tissue engineering: Present and future trends. *Virtual Phys. Prototyp.*, 2009, 4(4): 203–216
11. D. W. Huttmacher. Scaffolds in tissue engineering bone and cartilage. *Biomaterials*, 2000, 21(24): 2529–2543
12. D. Puppi, F. Chiellini, A. M. Piras, E. Chiellini. Polymeric materials for bone and cartilage repair. *Prog. Polym. Sci.*, 2010, 35(4): 403–440
13. H. Cao, N. Kuboyama. A biodegradable porous composite scaffold of PGA/ $\beta$ -TCP for bone tissue engineering. *Bone*, 2010, 46(2): 386–395
14. N. T. Khanarian, N. M. Haney, R. A. Burga, H. H. Lu. A functional agarose-hydroxyapatite scaffold for osteochondral interface regeneration. *Biomaterials*, 2012, 33(21): 5247–5258
15. F. P. W. Melchels, et al. The influence of the scaffold design on the distribution of adhering cells after perfusion cell seeding. *Biomaterials*, 2011, 32(11): 2878–2884
16. J. W. Lee, K. S. Kang, S. H. Lee, J. Y. Kim, B. K. Lee, D. W. Cho. Bone regeneration using a microstereolithography-produced customized poly(propylene fumarate)/diethyl fumarate photopolymer 3D scaffold incorporating BMP-2 loaded PLGA microspheres. *Biomaterials*, 2011, 32(3): 744–752
17. K. Kim, D. Dean, J. Wallace, R. Breithaupt, A. G. Mikos, J. P. Fisher. The influence of stereolithographic scaffold architecture and composition on osteogenic signal expression with rat bone marrow stromal cells. *Biomaterials*, 2011, 32(15): 3750–3763
18. P. Bajaj, R. M. Schweller, A. Khademhosseini, J. L. West, R. Bashir. 3D biofabrication strategies for tissue engineering and regenerative medicine. *Annu. Rev. Biomed. Eng.*, 2014, 16(1): 247–276
19. R. F. Pereira, P. J. Bártolo. Recent advances in additive biomanufacturing. In: S. H. Masood, ed. *Comprehensive Materials Processing, Volume 10: Advances in Additive Manufacturing and Tooling*. Oxford: Elsevier, 2014: 265–284
20. V. Mironov, R. P. Visconti, V. Kasyanov, G. Forgacs, C. J. Drake, R. R. Markwald. Organ printing: Tissue spheroids as building blocks. *Biomaterials*, 2009, 30(12): 2164–2174
21. J. W. Nichol, A. Khademhosseini. Modular tissue engineering: Engineering biological tissues from the bottom up. *Soft Matter*, 2009, 5(7): 1312–1319
22. S. V. Murphy, A. Atala. 3D bioprinting of tissues and organs. *Nat. Biotechnol.*, 2014, 32(8): 773–785
23. Y. B. Lee, et al. Bio-printing of collagen and VEGF-releasing fibrin gel scaffolds for neural stem cell culture. *Exp. Neurol.*, 2010, 223(2): 645–652
24. M. P. Lutolf. Materials science: Cell environments programmed with light. *Nature*, 2012, 482(7386): 477–478
25. K. T. Nguyen, J. L. West. Photopolymerizable hydrogels for tissue engineering applications. *Biomaterials*, 2002, 23(22): 4307–4314
26. I. Mironi-Harpaz, D. Y. Wang, S. Venkatraman, D. Seliktar. Photopolymerization of cell-encapsulating hydrogels: Crosslinking efficiency versus cytotoxicity. *Acta Biomater.*, 2012, 8(5): 1838–1848
27. C. A. DeForest, B. D. Polizzotti, K. S. Anseth. Sequential click reactions for synthesizing and patterning three-dimensional cell microenvironments. *Nat. Mater.*, 2009, 8(8): 659–664
28. K. A. Mosiewicz, et al. *In situ* cell manipulation through enzymatic hydrogel photopatterning. *Nat. Mater.*, 2013, 12(11): 1072–1078
29. R. F. Pereira, P. J. Bártolo. Photopolymerizable hydrogels in regenerative medicine and drug delivery. In: *Hot Topics in Biomaterials*. London: Future Science Ltd., 2014: 6–28
30. M. A. Azagarsamy, K. S. Anseth. Bioorthogonal click chemistry: An indispensable tool to create multifaceted cell culture scaffolds. *ACS Macro Lett.*, 2013, 2(1): 5–9
31. M. K. Nguyen, E. Alsberg. Bioactive factor delivery strategies from engineered polymer hydrogels for therapeutic medicine. *Prog. Polym. Sci.*, 2014, 39(7): 1235–1265
32. K. M. C. Tsang, et al. Facile one-step micropatterning using photodegradable gelatin hydrogels for improved cardiomyocyte organization and alignment. *Adv. Funct. Mater.*, 2015, 25(6): 977–986
33. F. Guillemot, et al. High-throughput laser printing of cells and biomaterials for tissue engineering. *Acta Biomater.*, 2010, 6(7): 2494–2500
34. C. C. Lin, C. S. Ki, H. Shih. Thiol-norbornene photo-click hydrogels for tissue engineering applications. *J. Appl. Polym. Sci.*, 2015, 132(8): 41563

35. N. Annabi, et al. 25th anniversary article: Rational design and applications of hydrogels in regenerative medicine. *Adv. Mater.*, 2014, 26(1): 85–124
36. S. B. Anderson, C. C. Lin, D. V. Kuntzler, K. S. Anseth. The performance of human mesenchymal stem cells encapsulated in cell-degradable polymer-peptide hydrogels. *Biomaterials*, 2011, 32(14): 3564–3574
37. F. R. Maia, K. B. Fonseca, G. Rodrigues, P. L. Granja, C. C. Barrias. Matrix-driven formation of mesenchymal stem cell-extracellular matrix microtissues on soft alginate hydrogels. *Acta Biomater.*, 2014, 10(7): 3197–3208
38. M. W. Tibbitt, A. M. Kloxin, L. Sawicki, K. S. Anseth. Mechanical properties and degradation of chain and step polymerized photodegradable hydrogels. *Macromolecules*, 2013, 46(7): 2785–2792
39. C. E. Hoyle, C. N. Bowman. Thiol-ene click chemistry. *Angew. Chem. Int. Ed. Engl.*, 2010, 49(9): 1540–1573
40. Y. Jiang, J. Chen, C. Deng, E. J. Suuronen, Z. Zhong. Click hydrogels, microgels and nanogels: Emerging platforms for drug delivery and tissue engineering. *Biomaterials*, 2014, 35(18): 4969–4985
41. M. A. Tasdelen, Y. Yagci. Light-induced click reactions. *Angew. Chem. Int. Ed. Engl.*, 2013, 52(23): 5930–5938
42. K. A. Kyburz, K. S. Anseth. Three-dimensional hMSC motility within peptide-functionalized PEG-based hydrogels of varying adhesivity and crosslinking density. *Acta Biomater.*, 2013, 9(5): 6381–6392
43. H. Shih, C. C. Lin. Visible-light-mediated thiol-ene hydrogelation using eosin-Y as the only photoinitiator. *Macromol. Rapid Commun.*, 2013, 34(3): 269–273
44. B. D. Fairbanks, M. P. Schwartz, A. E. Halevi, C. R. Nuttelman, C. N. Bowman, K. S. Anseth. A versatile synthetic extracellular matrix mimic via thiol-norbornene photopolymerization. *Adv. Mater.*, 2009, 21(48): 5005–5010
45. P. J. Bártolo. Stereolithographic processes. In: P. J. Bártolo, ed. *Stereolithography*. New York: Springer US, 2011: 1–36
46. N. E. Fedorovich, M. H. Oudshoorn, D. van Geemen, W. E. Hennink, J. Alblas, W. J. Dhert. The effect of photopolymerization on stem cells embedded in hydrogels. *Biomaterials*, 2009, 30(3): 344–353
47. A. D. Rouillard, et al. Methods for photocrosslinking alginate hydrogel scaffolds with high cell viability. *Tissue Eng. Part C Methods*, 2011, 17(2): 173–179
48. S. J. Bryant, C. R. Nuttelman, K. S. Anseth. Cytocompatibility of UV and visible light photoinitiating systems on cultured NIH/3T3 fibroblasts *in vitro*. *J. Biomater. Sci. Polym. Ed.*, 2000, 11(5): 439–457
49. C. G. Williams, A. N. Malik, T. K. Kim, P. N. Manson, J. H. Elisseeff. Variable cytocompatibility of six cell lines with photoinitiators used for polymerizing hydrogels and cell encapsulation. *Biomaterials*, 2005, 26(11): 1211–1218
50. T. Billiet, E. Gevaert, T. De Schryver, M. Cornelissen, P. Dubruel. The 3D printing of gelatin methacrylamide cell-laden tissue-engineered constructs with high cell viability. *Biomaterials*, 2014, 35(1): 49–62
51. B. D. Fairbanks, M. P. Schwartz, C. N. Bowman, K. S. Anseth. Photoinitiated polymerization of PEG-diacrylate with lithium phenyl-2,4,6-trimethylbenzoylphosphine: Polymerization rate and cytocompatibility. *Biomaterials*, 2009, 30(35): 6702–6707
52. Z. Li, et al. Initiation efficiency and cytotoxicity of novel water-soluble two-photon photoinitiators for direct 3D microfabrication of hydrogels. *RSC Adv.*, 2013, 3(36): 15939–15946
53. J. Hu, et al. Visible light crosslinkable chitosan hydrogels for tissue engineering. *Acta Biomater.*, 2012, 8(5): 1730–1738
54. J. W. Nichol, S. T. Koshy, H. Bae, C. M. Hwang, S. Yamanlar, A. Khademhosseini. Cell-laden microengineered gelatin methacrylate hydrogels. *Biomaterials*, 2010, 31(21): 5536–5544
55. W. M. Gramlich, I. L. Kim, J. A. Burdick. Synthesis and orthogonal photopatterning of hyaluronic acid hydrogels with thiol-norbornene chemistry. *Biomaterials*, 2013, 34(38): 9803–9811
56. A. Fu, K. Gwon, M. Kim, G. Tae, J. A. Kornfield. Visible-light-initiated thiol-acrylate photopolymerization of heparin-based hydrogels. *Biomacromolecules*, 2015, 16(2): 497–506
57. A. K. Nguyen, et al. Two-photon polymerization of polyethylene glycol diacrylate scaffolds with riboflavin and triethanolamine used as a water-soluble photoinitiator. *Regen. Med.*, 2013, 8(6): 725–738
58. H. Park, B. Choi, J. Hu, M. Lee. Injectable chitosan hyaluronic acid hydrogels for cartilage tissue engineering. *Acta Biomater.*, 2013, 9(1): 4779–4786
59. P. M. Kharkar, K. L. Kiick, A. M. Kloxin. Designing degradable hydrogels for orthogonal control of cell microenvironments. *Chem. Soc. Rev.*, 2013, 42(17): 7335–7372
60. J. A. Yang, J. Yeom, B. W. Hwang, A. S. Hoffman, S. K. Hahn. *In situ*-forming injectable hydrogels for regenerative medicine. *Prog. Polym. Sci.*, 2014, 39(12): 1973–1986
61. M. P. Lutolf, J. A. Hubbell. Synthetic biomaterials as instructive extracellular microenvironments for morphogenesis in tissue engineering. *Nat. Biotechnol.*, 2005, 23(1): 47–55
62. L. Fertier, et al. The use of renewable feedstock in UV-curable materials—A new age for polymers and green chemistry. *Prog. Polym. Sci.*, 2013, 38(6): 932–962
63. C. Heller, et al. Vinylcarbonates and vinylcarbamates: Biocompatible monomers for radical photopolymerization. *J. Polym. Sci. A Polym. Chem.*, 2011, 49(3): 650–661
64. B. Husár, R. Liska. Vinyl carbonates, vinyl carbamates, and related monomers: Synthesis, polymerization, and application. *Chem. Soc. Rev.*, 2012, 41(6): 2395–2405
65. C. Heller, M. Schwentenwein, G. Russmueller, F. Varga, J. Stampfl, R. Liska. Vinyl esters: Low cytotoxicity monomers for the fabrication of biocompatible 3D scaffolds by lithography based additive manufacturing. *J. Polym. Sci. A Polym. Chem.*, 2009, 47(24): 6941–6954
66. J. F. Almeida, P. Ferreira, A. Lopes, M. H. Gil. Photocrosslinkable biodegradable responsive hydrogels as drug delivery systems. *Int. J. Biol. Macromol.*, 2011, 49(5): 948–954
67. O. Jeon, C. Powell, L. D. Solorio, M. D. Krebs, E. Alsberg. Affinity-based growth factor delivery using biodegradable, photocrosslinked heparin-alginate hydrogels. *J. Control. Release*, 2011, 154(3): 258–266
68. S. Sahoo, C. Chung, S. Khetan, J. A. Burdick. Hydrolytically degradable hyaluronic acid hydrogels with controlled temporal structures. *Biomacromolecules*, 2008, 9(4): 1088–1092
69. S. A. Bencherif, A. Srinivasan, F. Horkay, J. O. Hollinger, K. Matyjaszewski, N. R. Washburn. Influence of the degree of methacrylation on hyaluronic acid hydrogels properties. *Biomaterials*, 2008, 29(12): 1739–1749
70. C. S. Ki, H. Shih, C. C. Lin. Facile preparation of photodegradable hydrogels by photopolymerization. *Polymer (Guildf.)*, 2013, 54(8): 2115–2122
71. Q. Guo, X. Wang, M. W. Tibbitt, K. S. Anseth, D. J. Montell, J. H. Elisseeff. Light activated cell migration in synthetic extracellular matrices. *Biomaterials*, 2012, 33(32): 8040–8046
72. M. A. Azagarsamy, D. D. McKinnon, D. L. Alge, K. S. Anseth. Coumarin-based photodegradable hydrogel: Design, synthesis, gelation, and degradation kinetics. *ACS Macro Letters*, 2014, 3(6): 515–519
73. M. A. Azagarsamy, K. S. Anseth. Wavelength-controlled photocleavage for the orthogonal and sequential release of multiple proteins. *Angew. Chem. Int. Ed. Engl.*, 2013, 52(51): 13803–13807
74. N. Annabi, S. M. Mithieux, P. Zorlutuna, G. Camci-Unal, A. S. Weiss, A.

- Khademhosseini. Engineered cell-laden human protein-based elastomer. *Biomaterials*, 2013, 34(22): 5496–5505
75. M. S. Bae, et al. Photo-cured hyaluronic acid-based hydrogels containing simvastatin as a bone tissue regeneration scaffold. *Biomaterials*, 2011, 32(32): 8161–8171
  76. H. Zhang, et al. Hyperbranched polyester hydrogels with controlled drug release and cell adhesion properties. *Biomacromolecules*, 2013, 14(5): 1299–1310
  77. Z. Muñoz, H. Shih, C. C. Lin. Gelatin hydrogels formed by orthogonal thiol-norbornene photochemistry for cell encapsulation. *Biomaterials Science*, 2014, 2(8): 1063–1072
  78. K. Peng, et al. Dextran based photodegradable hydrogels formed via a Michael addition. *Soft Matter*, 2011, 7(10): 4881–4887
  79. R. F. Pereira, H. A. Almeida, P. J. Bártolo. Biofabrication of hydrogel constructs. In: J. Coelho, ed. *Drug Delivery Systems: Advanced Technologies Potentially Applicable in Personalised Treatment*. Dordrecht: Springer Netherlands, 2013: 225–254
  80. N. R. Schiele, D. T. Corr, Y. Huang, N. A. Raof, Y. Xie, D. B. Chrisey. Laser-based direct-write techniques for cell printing. *Biofabrication*, 2010, 2(3): 032001
  81. F. P. W. Melchels, J. Feijen, D. W. Grijpma. A review on stereolithography and its applications in biomedical engineering. *Biomaterials*, 2010, 31(24): 6121–6130
  82. R. F. Pereira, P. J. Bártolo. Photocrosslinkable materials for the fabrication of tissue-engineered constructs by stereolithography. In: P. R. Fernandes, P. J. Bartolo, eds. *Tissue Engineering*. Dordrecht: Springer Netherlands, 2014: 149–178
  83. J. W. Choi, R. Wicker, S. H. Lee, K. H. Choi, C. S. Ha, I. Chung. Fabrication of 3D biocompatible/biodegradable micro-scaffolds using dynamic mask projection microstereolithography. *J. Mater. Process. Technol.*, 2009, 209(15–16): 5494–5503
  84. J. Torgersen, X. H. Qin, Z. Li, A. Ovsianikov, R. Liska, J. Stampfl. Hydrogels for two-photon polymerization: A toolbox for mimicking the extracellular matrix. *Adv. Funct. Mater.*, 2013, 23(36): 4542–4554
  85. P. J. Bártolo, G. Mitchell. Stereo-thermal-lithography: A new principle for rapid prototyping. *Rapid Prototyping J.*, 2003, 9(3): 150–156
  86. T. Patrício, R. Pereira, L. Oliveira, P. Bártolo. Polyethylene glycol and polyethylene glycol/hydroxyapatite constructs produced through stereo-thermal lithography. *Adv. Mater. Res.*, 2013, 749: 87–92
  87. P. Bartolo, et al. Biomedical production of implants by additive electrochemical and physical processes. *CIRP Annals—Manuf. Technol.*, 2012, 61(2): 635–655
  88. Y. J. Seol, D. Y. Park, J. Y. Park, S. W. Kim, S. J. Park, D. W. Cho. A new method of fabricating robust freeform 3D ceramic scaffolds for bone tissue regeneration. *Biotechnol. Bioeng.*, 2013, 110(5): 1444–1455
  89. J. R. Tumbleston, et al. Continuous liquid interface production of 3D objects. *Science*, 2015, 347(6228), 1349–1352
  90. S. J. Leigh, et al. Fabrication of 3-dimensional cellular constructs via microstereolithography using a simple, three-component, poly(ethylene glycol) acrylate-based system. *Biomacromolecules*, 2013, 14(1): 186–192
  91. A. P. Zhang, et al. Rapid fabrication of complex 3D extracellular microenvironments by dynamic optical projection stereolithography. *Adv. Mater.*, 2012, 24(31): 4266–4270
  92. A. Ovsianikov, et al. Laser fabrication of three-dimensional CAD scaffolds from photosensitive gelatin for applications in tissue engineering. *Biomacromolecules*, 2011, 12(4): 851–858
  93. K. W. Lee, S. Wang, B. C. Fox, E. L. Ritman, M. J. Yaszemski, L. Lu. Poly(propylene fumarate) bone tissue engineering scaffold fabrication using stereolithography: Effects of resin formulations and laser parameters. *Biomacromolecules*, 2007, 8(4): 1077–1084
  94. L. Elomaa, S. Teixeira, R. Hakala, H. Korhonen, D. W. Grijpma, J. V. Seppälä. Preparation of poly( $\epsilon$ -caprolactone)-based tissue engineering scaffolds by stereolithography. *Acta Biomater.*, 2011, 7(11): 3850–3856
  95. F. P. W. Melchels, J. Feijen, D. W. Grijpma. A poly(D,L-lactide) resin for the preparation of tissue engineering scaffolds by stereolithography. *Biomaterials*, 2009, 30(23–24): 3801–3809
  96. S. Schüller-Ravoo, S. M. Teixeira, J. Feijen, D. W. Grijpma, A. A. Poot. Flexible and elastic scaffolds for cartilage tissue engineering prepared by stereolithography using poly(trimethylene carbonate)-based resins. *Macromol. Biosci.*, 2013, 13(12): 1711–1719
  97. J. W. Lee, P. X. Lan, B. Kim, G. Lim, D. W. Cho. Fabrication and characteristic analysis of a poly(propylene fumarate) scaffold using microstereolithography technology. *J. Biomed. Mater. Res. B Appl. Biomater.*, 2008, 87B(1): 1–9
  98. J. Jansen, F. P. Melchels, D. W. Grijpma, J. Feijen. Fumaric acid monoethyl ester-functionalized poly(D,L-lactide)/N-vinyl-2-pyrrolidone resins for the preparation of tissue engineering scaffolds by stereolithography. *Biomacromolecules*, 2009, 10(2): 214–220
  99. T. M. Seck, F. P. Melchels, J. Feijen, D. W. Grijpma. Designed biodegradable hydrogel structures prepared by stereolithography using poly(ethylene glycol)/poly(D,L-lactide)-based resins. *J. Control. Release*, 2010, 148(1): 34–41
  100. K. Arcaute, B. Mann, R. Wicker. Stereolithography of spatially controlled multi-material bioactive poly(ethylene glycol) scaffolds. *Acta Biomater.*, 2010, 6(3): 1047–1054
  101. F. A. M. M. Gonçalves, et al. 3D printing of new biobased unsaturated polyesters by microstereo-thermal-lithography. *Biofabrication*, 2014, 6(3): 035024
  102. M. Dadsetan, et al. Effect of calcium phosphate coating and rhBMP-2 on bone regeneration in rabbit calvaria using poly(propylene fumarate) scaffolds. *Acta Biomater.*, 2015 (in press)
  103. J. H. Shin, J. W. Lee, J. H. Jung, D. W. Cho, G. Lim. Evaluation of cell proliferation and differentiation on a poly(propylene fumarate) 3D scaffold treated with functional peptides. *J. Mater. Sci.*, 2011, 46(15): 5282–5287
  104. L. Elomaa, Y. Kang, J. V. Seppälä, Y. Yang. Biodegradable photocrosslinkable poly(depsipeptide-co- $\epsilon$ -caprolactone) for tissue engineering: Synthesis, characterization, and *in vitro* evaluation. *J. Polym. Sci. A Polym. Chem.*, 2014, 52(23): 3307–3315
  105. R. Gauvin, et al. Microfabrication of complex porous tissue engineering scaffolds using 3D projection stereolithography. *Biomaterials*, 2012, 33(15): 3824–3834
  106. F. Scalera, C. Esposito Corcione, F. Montagna, A. Sannino, A. Maffezzoli. Development and characterization of UV curable epoxy/hydroxyapatite suspensions for stereolithography applied to bone tissue engineering. *Ceram. Int.*, 2014, 40(10, Part A): 15455–15462
  107. L. Elomaa, A. Kokkari, T. Närhi, J. V. Seppälä. Porous 3D modeled scaffolds of bioactive glass and photocrosslinkable poly( $\epsilon$ -caprolactone) by stereolithography. *Compos. Sci. Technol.*, 2013, 74: 99–106
  108. A. Ronca, L. Ambrosio, D. W. Grijpma. Preparation of designed poly(D,L-lactide)/nanosized hydroxyapatite composite structures by stereolithography. *Acta Biomater.*, 2013, 9(4): 5989–5996
  109. F. Claeysens, et al. Three-dimensional biodegradable structures fabricated by two-photon polymerization. *Langmuir*, 2009, 25(5): 3219–3223
  110. O. Kufelt, A. El-Tamer, C. Sehring, S. Schlie-Wolter, B. N. Chichkov. Hyaluronic acid based materials for scaffolding via two-photon polymerization. *Biomacromolecules*, 2014, 15(2): 650–659

111. V. Melissinaki, et al. Direct laser writing of 3D scaffolds for neural tissue engineering applications. *Biofabrication*, 2011, 3(4): 045005
112. M. T. Raimondi, et al. Three-dimensional structural niches engineered via two-photon laser polymerization promote stem cell homing. *Acta Biomater.*, 2013, 9(1): 4579–4584
113. J. W. Lee, K. J. Kim, K. S. Kang, S. Chen, J. W. Rhie, D. W. Cho. Development of a bone reconstruction technique using a solid free-form fabrication (SFF)-based drug releasing scaffold and adipose-derived stem cells. *J. Biomed. Mater. Res. A*, 2013, 101A(7): 1865–1875
114. J. Jansen, M. J. Boerakker, J. Heuts, J. Feijen, D. W. Grijpma. Rapid photo-crosslinking of fumaric acid monoethyl ester-functionalized poly(trimethylene carbonate) oligomers for drug delivery applications. *J. Control. Release*, 2010, 147(1): 54–61
115. S. D. Gittard, et al. Two photon polymerization-micromolding of polyethylene glycol-gentamicin sulfate microneedles. *Adv. Eng. Mater.*, 2010, 12(4): B77–B82
116. S. D. Gittard, et al. Deposition of antimicrobial coatings on microstereolithography-fabricated microneedles. *JOM*, 2011, 63(6): 59–68
117. Y. Lu, G. Mapili, G. Suhali, S. Chen, K. Roy. A digital micro-mirror device-based system for the microfabrication of complex, spatially patterned tissue engineering scaffolds. *J. Biomed. Mater. Res. A*, 2006, 77A(2): 396–405
118. P. Zorlutuna, J. H. Jeong, H. Kong, R. Bashir. Stereolithography-based hydrogel microenvironments to examine cellular interactions. *Adv. Funct. Mater.*, 2011, 21(19): 3642–3651
119. V. Chan, P. Zorlutuna, J. H. Jeong, H. Kong, R. Bashir. Three-dimensional photopatterning of hydrogels using stereolithography for long-term cell encapsulation. *Lab Chip*, 2010, 10(16): 2062–2070
120. H. Lin, et al. Application of visible light-based projection stereolithography for live cell-scaffold fabrication with designed architecture. *Biomaterials*, 2013, 34(2): 331–339
121. A. Ovsianikov, et al. Laser photofabrication of cell-containing hydrogel constructs. *Langmuir*, 2014, 30(13): 3787–3794
122. A. Ovsianikov, et al. Laser printing of cells into 3D scaffolds. *Biofabrication*, 2010, 2(1): 014104
123. Y. Nahmias, D. J. Odde. Micropatterning of living cells by laser-guided direct writing: Application to fabrication of hepatic-endothelial sinusoid-like structures. *Nat. Protoc.*, 2006, 1(5): 2288–2296
124. B. R. Ringeisen, C. M. Othon, J. A. Barron, P. K. Wu, B. J. Spargo. The evolution of cell printing. In: U. Meyer, J. Handschel, H. P. Wiesmann, T. Meyer, eds. *Fundamentals of Tissue Engineering and Regenerative Medicine*. Berlin: Springer Berlin Heidelberg, 2009: 613–631
125. D. J. Odde, M. J. Renn. Laser-guided direct writing of living cells. *Biotechnol. Bioeng.*, 2000, 67(3): 312–318
126. Y. Nahmias, R. E. Schwartz, C. M. Verfaillie, D. J. Odde. Laser-guided direct writing for three-dimensional tissue engineering. *Biotechnol. Bioeng.*, 2005, 92(2): 129–136
127. F. Guillemot, A. Souquet, S. Catros, B. Guillotin. Laser-assisted cell printing: Principle, physical parameters versus cell fate and perspectives in tissue engineering. *Nanomedicine (Lond)*, 2010, 5(3): 507–515
128. S. Catros, B. Guillotin, M. Bačáková, J. C. Fricain, F. Guillemot. Effect of laser energy, substrate film thickness and bioink viscosity on viability of endothelial cells printed by Laser-Assisted Bioprinting. *Appl. Surf. Sci.*, 2011, 257(12): 5142–5147
129. J. A. Barron, D. B. Krizman, B. R. Ringeisen. Laser printing of single cells: Statistical analysis, cell viability, and stress. *Ann. Biomed. Eng.*, 2005, 33(2): 121–130
130. Y. Lin, G. Huang, Y. Huang, T. R. Jeremy Tzeng, D. Chrisey. Effect of laser fluence in laser-assisted direct writing of human colon cancer cell. *Rapid Prototyping J.*, 2010, 16(3): 202–208
131. B. C. Riggs, et al. Matrix-assisted pulsed laser methods for biofabrication. *MRS Bull.*, 2011, 36(12): 1043–1050
132. N. A. Raof, N. R. Schiele, Y. Xie, D. B. Chrisey, D. T. Corr. The maintenance of pluripotency following laser direct-write of mouse embryonic stem cells. *Biomaterials*, 2011, 32(7): 1802–1808
133. J. A. Barron, B. R. Ringeisen, H. Kim, B. J. Spargo, D. B. Chrisey. Application of laser printing to mammalian cells. *Thin Solid Films*, 2004, 453–454: 383–387
134. T. M. Patz, et al. Three-dimensional direct writing of B35 neuronal cells. *J. Biomed. Mater. Res. B Appl. Biomater.*, 2006, 78B(1): 124–130
135. N. R. Schiele, D. B. Chrisey, D. T. Corr. Gelatin-based laser direct-write technique for the precise spatial patterning of cells. *Tissue Eng. Part C Methods*, 2011, 17(3): 289–298
136. N. R. Schiele, et al. Laser direct writing of combinatorial libraries of idealized cellular constructs: Biomedical applications. *Appl. Surf. Sci.*, 2009, 255(10): 5444–5447
137. A. Doraiswamy, R. J. Narayan, M. L. Harris, S. B. Qadri, R. Modi, D. B. Chrisey. Laser microfabrication of hydroxyapatite-osteoblast-like cell composites. *J. Biomed. Mater. Res. A*, 2007, 80A(3): 635–643
138. S. Catros, et al. Laser-assisted bioprinting for creating on-demand patterns of human osteoprogenitor cells and nano-hydroxyapatite. *Biofabrication*, 2011, 3(2): 025001
139. M. Gruene, et al. Laser printing of three-dimensional multicellular arrays for studies of cell-cell and cell-environment interactions. *Tissue Eng. Part C Methods*, 2011, 17(10): 973–982
140. L. Koch, et al. Skin tissue generation by laser cell printing. *Biotechnol. Bioeng.*, 2012, 109(7): 1855–1863
141. P. K. Wu, B. R. Ringeisen. Development of human umbilical vein endothelial cell (HUVEC) and human umbilical vein smooth muscle cell (HUVSMC) branch/stem structures on hydrogel layers via biological laser printing (BioLP). *Biofabrication*, 2010, 2(1): 014111
142. S. Michael, et al. Tissue engineered skin substitutes created by laser-assisted bioprinting form skin-like structures in the dorsal skin fold chamber in mice. *PLoS ONE*, 2013, 8(3): e57741
143. V. Keriquel, et al. *In vivo* bioprinting for computer- and robotic-assisted medical intervention: Preliminary study in mice. *Biofabrication*, 2010, 2(1): 014101
144. B. Guillotin, et al. Laser-assisted bioprinting for tissue engineering. In: G. Forgacs, W. Sun, eds. *Biofabrication*. Boston: William Andrew Publishing, 2013: 95–118
145. R. G. Wylie, S. Ahsan, Y. Aizawa, K. L. Maxwell, C. M. Morshead, M. S. Shoichet. Spatially controlled simultaneous patterning of multiple growth factors in three-dimensional hydrogels. *Nat. Mater.*, 2011, 10(10): 799–806
146. R. G. Wylie, M. S. Shoichet. Three-dimensional spatial patterning of proteins in hydrogels. *Biomacromolecules*, 2011, 12(10): 3789–3796
147. S. H. Lee, J. J. Moon, J. L. West. Three-dimensional micropatterning of bioactive hydrogels via two-photon laser scanning photolithography for guided 3D cell migration. *Biomaterials*, 2008, 29(20): 2962–2968
148. S. C. Owen, S. A. Fisher, R. Y. Tam, C. M. Nimmo, M. S. Shoichet. Hyaluronic acid click hydrogels emulate the extracellular matrix. *Langmuir*, 2013, 29(24): 7393–7400
149. K. A. Mosiewicz, L. Kolb, A. J. van der Vlies, M. P. Lutolf. Microscale patterning of hydrogel stiffness through light-triggered uncaging of thiols. *Biomater. Sci.*, 2014, 2(11): 1640–1651
150. A. T. Alsop, J. C. Pence, D. W. Weisgerber, B. A. Harley, R. C. Bailey. Photopatterning of vascular endothelial growth factor within collagen-

- glycosaminoglycan scaffolds can induce a spatially confined response in human umbilical vein endothelial cells. *Acta Biomater.*, 2014, 10(11): 4715–4722
151. R. J. Wade, E. J. Bassin, W. M. Gramlich, J. A. Burdick. Nanofibrous hydrogels with spatially patterned biochemical signals to control cell behavior. *Adv. Mater.*, 2015, 27(8): 1356–1362
  152. H. J. Lee, W. G. Koh. Hydrogel micropattern-incorporated fibrous scaffolds capable of sequential growth factor delivery for enhanced osteogenesis of hMSCs. *ACS Appl. Mater. Interfaces*, 2014, 6(12): 9338–9348
  153. B. V. Sridhar, N. R. Doyle, M. A. Randolph, K. S. Anseth. Covalently tethered TGF- $\beta$ 1 with encapsulated chondrocytes in a PEG hydrogel system enhances extracellular matrix production. *J. Biomed. Mater. Res. A*, 2014, 102(12): 4464–4472
  154. G. Pasparakis, T. Manouras, P. Argitis, M. Vamvakaki. Photodegradable polymers for biotechnological applications. *Macromol. Rapid Commun.*, 2012, 33(3): 183–198
  155. M. T. Frey, Y. L. Wang. A photo-modulatable material for probing cellular responses to substrate rigidity. *Soft Matter*, 2009, 5(9): 1918–1924
  156. V. V. Ramanan, J. S. Katz, M. Guvendiren, E. R. Cohen, R. A. Marklein, J. A. Burdick. Photocleavable side groups to spatially alter hydrogel properties and cellular interactions. *J. Mater. Chem.*, 2010, 20(40): 8920–8926
  157. D. R. Griffin, A. M. Kasko. Photodegradable macromers and hydrogels for live cell encapsulation and release. *J. Am. Chem. Soc.*, 2012, 134(31): 13103–13107
  158. D. R. Griffin, J. T. Patterson, A. M. Kasko. Photodegradation as a mechanism for controlled drug delivery. *Biotechnol. Bioeng.*, 2010, 107(6): 1012–1019
  159. M. He, J. Li, S. Tan, R. Wang, Y. Zhang. Photodegradable supramolecular hydrogels with fluorescence turn-on reporter for photomodulation of cellular microenvironments. *J. Am. Chem. Soc.*, 2013, 135(50): 18718–18721
  160. C. A. DeForest, K. S. Anseth. Cytocompatible click-based hydrogels with dynamically tunable properties through orthogonal photoconjugation and photocleavage reactions. *Nat. Chem.*, 2011, 3(12): 925–931
  161. A. M. Kloxin, J. A. Benton, K. S. Anseth. *In situ* elasticity modulation with dynamic substrates to direct cell phenotype. *Biomaterials*, 2010, 31(1): 1–8
  162. C. M. Kirschner, D. L. Alge, S. T. Gould, K. S. Anseth. Clickable, photodegradable hydrogels to dynamically modulate valvular interstitial cell phenotype. *Adv. Healthc. Mater.*, 2014, 3(5): 649–657
  163. M. V. Tsurkan, et al. Photopatterning of multifunctional hydrogels to direct adult neural precursor cells. *Adv. Healthc. Mater.*, 2015, 4(4): 516–521
  164. M. A. Azagarsamy, D. L. Alge, S. J. Radhakrishnan, M. W. Tibbitt, K. S. Anseth. Photocontrolled nanoparticles for on-demand release of proteins. *Biomacromolecules*, 2012, 13(8): 2219–2224
  165. M. W. Tibbitt, B. W. Han, A. M. Kloxin, K. S. Anseth. Synthesis and application of photodegradable microspheres for spatiotemporal control of protein delivery. *J. Biomed. Mater. Res. A*, 2012, 100A(7): 1647–1654
  166. C. Lv, Z. Wang, P. Wang, X. Tang. Photodegradable polyurethane self-assembled nanoparticles for photocontrollable release. *Langmuir*, 2012, 28(25): 9387–9394
  167. J. L. Vivero-Escoto, I. I. Slowing, C. W. Wu, V. S. Lin. Photoinduced intracellular controlled release drug delivery in human cells by gold-capped mesoporous silica nanosphere. *J. Am. Chem. Soc.*, 2009, 131(10): 3462–3463
  168. Q. Jin, F. Mitschang, S. Agarwal. Biocompatible drug delivery system for photo-triggered controlled release of 5-fluorouracil. *Biomacromolecules*, 2011, 12(10): 3684–3691
  169. B. Yan, J. C. Boyer, D. Habault, N. R. Branda, Y. Zhao. Near infrared light triggered release of biomacromolecules from hydrogels loaded with up-conversion nanoparticles. *J. Am. Chem. Soc.*, 2012, 134(40): 16558–16561